The synthesis and biological applications of photo-activated ruthenium anticancer drugs

Lameijer, L.N.

Chapter 5:

$[Ru(phbpy)(N\text{-}N)(dmso\text{-}\kappa S)]^+$

A new photo-active chiral cyclometalated analogue of the $Ru(tpy)(N\text{-}N)(dmso\text{-}kS)^{2+}$ scaffold

Abstract: Herein the synthesis of five new cyclometalated complexes with the general formula $[Ru(phbpy)(N\text{-}N)(dmso\text{-}\kappa S)]^+$ is described, where Hphbpy = 6'-phenyl-2,2'-bipyridyl, N-N = bpy (2,2'-bipyridine), phen (1,10-phenanthroline), dpq (pyrazino[2,3-*f*][1,10]phenanthroline), dppz (dipyrido[3,2-*a*:2',3'-*c*]phenazine or dppn (benzo[*i*]dipyrido[3,2-*a*:2',3'-*c*]phenazine). The thermal and photophysical properties of these complexes is investigated. The photosubstitution of dmso (Φ_{450} = 4.1 x 10^{-5} for $[Ru(phbpy)(bpy)(dmso\text{-}\kappa S)]^+$ and Φ_{450} = 1.6 x 10^{-2} $[Ru(phbpy)(bpy)(dmso\text{-}\kappa S)]^+$) or the absence of photodissociation ($[Ru(phbpy)(dppz)(dmso\text{-}\kappa S)]^+$ and $[Ru(phbpy)(dppn)(dmso\text{-}\kappa S)]^+$) is explained in comparison to their polypyridyl analogues using electrochemistry and density functional theory (DFT) calculations. Their photoreactivity further translates to their cytotoxic properties against two different cancer cells lines (A549, lung cancer and MCF-7, breast cancer): Depending on the structure of the bidentate ligand, the complexes are photocytotoxic towards cancer cells using green light (11 µM before and 2 µM after irradiation when N-N = dpq) or highly cytotoxic in the dark (0.51 µM when N-N = dppn). Furthermore, by exploiting the photolability of $[Ru(phbpy)(phen)(dmso\text{-}\kappa S)]PF_6$ it was possible to separate the two enantiomers of this chiral molecule by coordination of a chiral sulfoxide followed by chiral HPLC purification. Therefore providing a new approach towards the synthesis of chiral cyclometalated ruthenium(II) complexes.

This chapter will be submitted for publication: L. N. Lameijer, C. J. van de Griend, A. G. Volbeda, M. A. Siegler, S. Bonnet; *Manuscript in preparation.*

5.1 Introduction

Since the clinical approval of cisplatin a great leap forward has been made in the field of bio-inorganic chemistry leading to the discovery of many new ruthenium complexes with anticancer properties. Two of the most thoroughly investigated anti-cancer agents are NAMI-A and KP1339 for which the latter clinical research is still ongoing. Currently, most research is focused on either compounds based upon the piano-stool Ru(II)η^6-arene scaffold pioneered by the groups of Dyson and Sadler,[1] or ruthenium(II) polypyridyl complexes, of which several (photoactive) candidates have been developed by the groups of Dunbar,[2] Gasser,[3] Glazer,[4] Renfrew[5] and Turro.[6] More recently cyclometalated analogues of these complexes have emerged as a new subclass of light-activatable anticancer complexes.[2] Typically, in this type of compounds one nitrogen atom in a polypyridyl ligand has been replaced by a carbon atom, resulting in an organometallic metallacycle.[7] As a consequence, cyclometalated compounds often have better properties for chemotherapy or photodynamic therapy (PDT) than their non-cyclometalated analogons.[7] In particular, cyclometalation leads to an increase in lipophilicity due to the decrease in the charge of the complex, which in turn increases uptake in cancer cells[8] and often leads to higher cytotoxicity[9] towards cancer cells. In addition, cycloruthenated polypyridyl complexes demonstrate to have more interesting properties for phototherapy compared to their non-cyclometalated analogons. Whereas the latter class of compounds typically absorb between 400 and 600 nm,[10] a bathochromic shift is often observed for cyclometalated compounds due to the destabilization of t_{2g} orbitals by the π-donating cyclometalated carbanionic ligand, potentially allowing activation of these compounds with red light.[11] The group of Turro has previously reported two cyclometalated complexes, *cis*-[Ru(phpy)(phen)(MeCN)$_2$]PF$_6$ and *cis*-[Ru(phpy)(bpy)(MeCN)$_2$]PF$_6$, (phpy = 2-phenylpyridine) that are capable of photosubstituting their acetonitrile ligand, and are phototoxic in cancer cells.[12] Inspired by this work and following up on our investigation of caged ruthenium complexes with the general formula [Ru(tpy)(N-N)(L)]$^{2+}$ in which L is a sulfur-based ligand, we herein investigate the synthesis, photochemistry, and biological properties of these complexes in which a carbanion is introduced in the tridentate ligand. Complexes [**1**]PF$_6$-[**5**]PF$_6$ have the general formula [Ru(phbpy)(N-N)(dmso-κS)]PF$_6$ with Hphbpy = 6'-phenyl-2,2'-bipyridyl and N-N = bpy (2,2'-bipyridine, [**1**]PF$_6$), phen (1,10-phenanthroline, [**2**]PF$_6$), dpq (pyrazino[2,3-*f*][1,10]phenanthroline, [**3**]PF$_6$), dppz (dipyrido[3,2-*a*:2',3'-*c*]phenazine), [**4**]PF$_6$), and dppn (benzo[*i*]dipyrido[3,2-*a*:2',3'-*c*]phenazine, [**5**]PF$_6$). An interesting property of these complexes is their chirality: By replacing one nitrogen atom in the tridentate ligand the plane of symmetry of these complexes is lost, effectively resulting in a chiral scaffold. In this chapter we elaborate on this new class of compounds, by providing insight in their synthesis, photophysical properties and compare their photoreactivity with that of the [Ru(tpy)(N-N)(L)]$^{2+}$ complexes described in chapter 4. Furthermore, we demonstrate the

different ligand exchange properties of these complexes and answer the question whether these chiral complexes can be resolved, i.e., if their enantiomers can be separated.

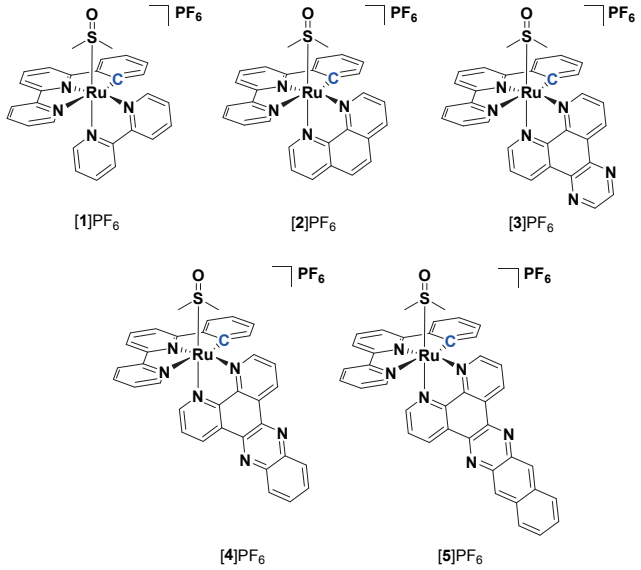

Figure 5.1. Chemical structures of the complexes presented in this study. $[Ru(phbpy)(NN)(dmso\text{-}\kappa S)]^+$, where N-N = bpy, phen, dpq, dppz or dppn.

5.2 Results

5.2.1 Synthesis

The first attempted route towards the synthesis of compounds [**1**]PF_6 – [**5**]PF_6 (Figure 5.1), inspired by the report of Ryabov and coworkers,[13] consisted in the coordination of the terpyridine analogon Hphbpy to the ruthenium benzene dimer $[(\eta^6\text{-}C_6H_6)RuCl(\mu\text{-}Cl)]_2$. However, this approach afforded the intermediate species $[Ru(phbpy)(MeCN)_3]PF_6$ in a maximum yield of only 32% and proved to be difficult to scale up. Therefore triggering the search for an alternative route depicted in Scheme 1. Starting from *cis*-$[RuCl_2(dmso\text{-}\kappa S)_3(dmso\text{-}\kappa O)]$, the reaction of the bidentate ligand N-N = bpy, phen, dpq, dppz, or dppn, was realized first, followed by cyclometalation using Hphbpy in the presence of a catalytic amount of *N*-methylmorpholine, affording the five compounds $[Ru(phbpy)(N\text{-}N)(dmso\text{-}\kappa S)]PF_6$ ([**1**]PF_6 – [**5**]PF_6) as a racemic mixture of enantiomers in good yield (65 – 74%).

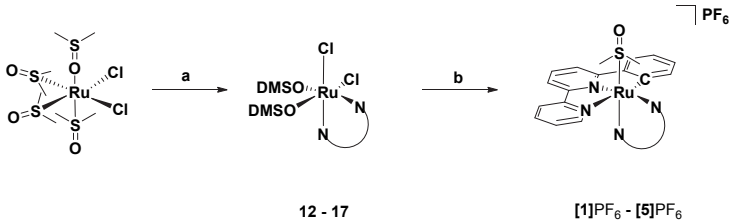

Scheme 5.1. Reagents and conditions. a). N-N = bpy in EtOH/DMSO (1:15), reflux, 86%; b). Phbpy, cat. *N*-methylmorpholine in MeOH/H_2O (5:1), reflux, 65%. For N-N = phen = 77% and 68%, N-N = dpq = 95% and 74%, NN = dppz = 87% and 73%, NN = dppn = 96% and 65%.

With these compounds in hand, we attempted to obtain diastereomers by the thermal reaction of several chiral ligands as shown in Scheme 2 and summarized in Table 5.1 (entry 1 – 6). Heating [**1**]PF_6 and (R)-methyl p-tolylsulfoxide at increased temperatures (120 °C) in DMF resulted in the formation of ruthenium(III) species, as observed by a green color, whereas lower temperatures only led to the recovery of starting materials. Further attempts to substitute the monodentate ligand with non-chiral ligands (entry 7 – 8) such as LiCl, pyridine and acetonitrile also proved unsuccessful. This inertness is exceptional, as the terpyridine analogues of these complexes are known to thermally engage into selective exchange of the monodentate ligand in similar or milder conditions.[14] The only thermal substitution observed with [**4**]$(PF_6)_2$ was achieved in acetic acid, which resulted in the partial formation of $[Ru(phbpy)(dppz)(AcOH)]^+$ as proven by mass spectrometry (found m/z 675.1, calcd. m/z 675.1), although this compound could not be isolated.

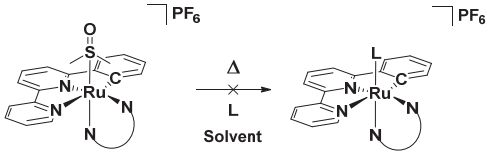

Scheme 5.2. General approach for the thermal conversion of complexes [**1**]PF_6, [**2**]PF_6 and [**4**]PF_6 with different monodentate ligands L.

Table 5.1. Attempts of ligand exchange for [**1**]PF_6, [**2**]PF_6 and [**4**]PF_6.

Entry	Complex	Ligand (L)	Solvent	T (°C)	Substitution
1	[**1**]PF_6	(*R*)-Methyl *p*-tolylsulfoxide (5 eq.)	DMF	120	-
2	[**1**]PF_6	(*R*)-Methyl *p*-tolylsulfoxide (5 eq.)	DMF	80	-
3	[**1**]PF_6	(*R*)-Methyl *p*-tolylsulfoxide (5 eq.)	EtOH 3:1 H_2O	80	-
4	[**4**]PF_6	Biotin (20 eq.)	EtOH 3:1 H_2O	80	-
5	[**4**]PF_6	N-acetyl-L-methionine (20 eq.)	EtOH 3:1 H_2O	80	-
6	[**4**]PF_6	N-Acetyl-L-cysteine methyl ester (20 eq.)	EtOH 3:1 H_2O	80	-
7	[**4**]PF_6	L-Histidine methyl ester 2HCl (20 eq.)	EtOH 3:1 H_2O	80	-
8	[**2**]PF_6	LiCl (20 eq.)	EtOH 3:1 H_2O	80	-
9	[**4**]PF_6	-	MeCN	80	-
10	[**4**]PF_6	-	Pyridine	80	-
11	[**4**]PF_6	-	Acetic acid	80	Yes

5.2.2 Crystal structures

Single crystals suitable for crystal structure determination were obtained by slow vapor diffusion of ethyl acetate in dichloromethane for [**1**]PF_6, hexane in DCM for [**2**]PF_6 and [**3**]PF_6, or slow evaporation of a solution of [**4**]PF_6 in toluene. All compounds crystallized in space groups having an inversion center, thus containing a (1:1) mixture of enantiomers. A selection of bond lengths and angles is shown in Table 5.2. As expected, the ruthenium centers in these compounds have a distorted octahedral geometry similar to that of their terpyridyl analogues (described in chapter 4). Compared to [Ru(tpy)(bpy)(dmso-κS)]$(OTf)_2$ replacing the nitrogen within this scaffold with an anionic carbon atom has only a modest effect on the bond length of Ru1-C1 (2.043 Å) in [**1**]PF_6 compared to Ru1-N1 (2.079 Å).[15] Furthermore, compared to its non-cyclometalated analogon the *trans-influence* of the carbon atom in phbpy$^-$ results in an elongation of the Ru1-N2 bond length in $[Ru(phbpy)(bpy)(dmso\text{-}\kappa S)]^{2+}$ (2.173(2) Å), whereas in $[Ru(tpy)(bpy)(dmso\text{-}\kappa S)]^{2+}$ the Ru1-N3 length is 2.079(2) Å.[16] In contrast, the ruthenium-sulfur bond length is shorter in [**1**]PF_6 (2.2558(7) Å) than in $[Ru(tpy)(bpy)(dmso\text{-}\kappa S)]^{2+}$ (2.282(1) Å) as a result of the increased electron density on ruthenium, leading to stronger backbonding into the π* orbital of the S-bound dmso ligand. Overall, this electronic effect barely affects the angles between C1-Ru1-N3 for [**1**]PF_6 (158.67(12) Å) and N1-Ru1-N3 for $[Ru(tpy)(bpy)(dmso\text{-}\kappa S)]^{2+}$ (157.92(8) Å), confirming their high structural similarity.

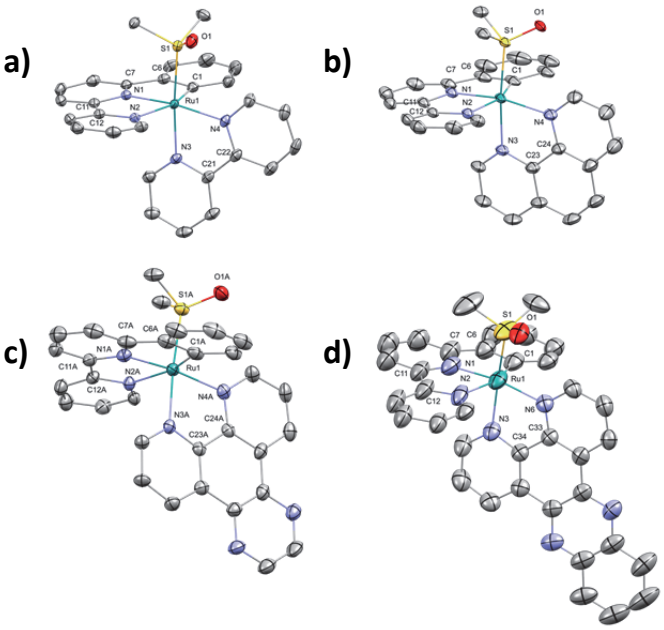

Figure 5.2. Displacement ellipsoid plots (50% probability level) of the cationic part of the crystal structure of [**1**]PF_6 (a), [**2**]PF_6 (b), [**3**]PF_6 (c) and [**4**]PF_6 (d). Hydrogen atom and counter ions have been omitted for clarity.

Table 5.2. Selected bond distances (Å) and bond angles (°) for complexes [**1**]PF_6, [**2**]PF_6, [**3**]PF_6 and [**4**]PF_6.

	[**1**]PF_6	[**2**]PF_6	[**3**]PF_6	[**4**]PF_6
Ru1-S1	2.2558(7)	2.2359(4)	2.2405(9)	2.210(3)
Ru1-C1	2.043(2)	2.041(3)	2.029(5)	2.030(1)
Ru1-N1	2.002(2)	2.004(2)	2.005(5)	2.019(7)
Ru1-N2	2.173(2)	2.164(2)	2.176(3)	2.180(1)
Ru1-N3	2.088(2)	2.110(2)	2.089(3)	2.094(3)
Ru1-N4	2.079(2)	2.091(2)	2.083(4)	2.071(4)
S1-O1	1.486(2)	1.489(2)	1.485(3)	1.501(6)
C1-Ru1-N2	157.92(8)	158.45(9)	158.5(2)	155.6(7)
N3-Ru1-N4	78.07(7)	78.67(7)	78.9(1)	78.2(1)
S1-Ru1-N4	96.25(5)	97.29(5)	96.6(1)	96.0(1)

5.2.3 Electronic absorption, emission and singlet oxygen

Electronic absorption spectra were recorded in acetonitrile for complexes [**1**]PF_6 – [**5**]PF_6 (Figure 5.3a) and the acetonitrile substituted $[Ru(phbpy)(N\text{-}N)(CD_3CN)]^{2+}$ derivatives [**6**]PF_6, [**7**]PF_6 and [**8**]PF_6 (Figure 5.3b, for synthesis, see below). $[Ru(tpy)(bpy)(dmso\text{-}\kappa S)](PF_6)_2$, [**9**]$(PF_6)_2$ and $[Ru(tpy)(bpy)(MeCN)](PF_6)_2$, [**10**]$(PF_6)_2$ are included to demonstrate the effect of the $phbpy^-$ ligand on the absorption spectra of the cyclometalated complexes. Compounds [**1**]PF_6 – [**5**]PF_6 showed a considerable bathochromic shift (~40 nm, Table 5.3) and have a broader ^{1}MLCT band compared to [**9**]$(PF_6)_2$ (411 nm, Table 5.3). Similarly, the photoproducts for [**1**]PF_6 – [**3**]PF_6 in acetonitrile show a comparable shift of approximately 50 nm compared to [**10**]$(PF_6)_2$. Such a bathochromic shift is common for cyclometalated ruthenium analogues as reported in literature,[16-17] and it is mostly ascribed to an increase in the energy of the highest occupied molecular orbital (HOMO) since the lowest unoccupied molecular orbital (LUMO) remains relatively unchanged.[16] Furthermore, for [**4**]PF_6 and [**5**]PF_6 near-UV and visible ligand-based π-π^* transitions are also observed around 370 nm and 410 nm respectively, due to the increased conjugation of the dppz and dppn ligands.

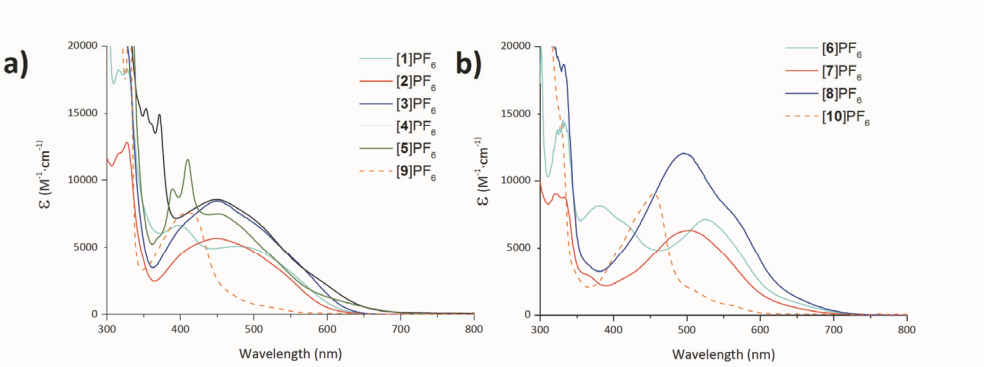

Figure 5.3 a). Electronic absorption spectra for [**1**]PF_6 – [**5**]PF_6 and b). [**6**]PF_6 – [**8**]PF_6 in acetonitrile. Dashed lines are for non-cyclometalated analogons [**9**]$(PF_6)_2$ and [**10**]$(PF_6)_2$ respectively.

Emission was measured for complexes [**1**]PF_6 – [**5**]PF_6 in acetonitrile. The maxima are reported in Table 5.3. All compounds are very weakly emissive with a slightly higher phosphorescence quantum yield (Φ_p) compared to the cyclometalated analogon $[Ru(phbpy)(tpy)]^+$ ($\Phi_P = 5 \cdot 10^{-6}$).[18] The emission wavelengths found for [**1**]PF_6 – [**3**]PF_6 are

comparable to those of $[Ru(phbpy)(tpy)]^+$ (786 – 800 nm versus 797 nm)[18] and are similar to complexes reported by the group of Turro and Sauvage.[16, 18] For complexes [**4**]PF_6 and [**5**]PF_6 a blue-shifted emission (618 and 672 nm) was observed compared to $[Ru(phbpy)(tpy)]^+$. Singlet oxygen quantum yields (Φ_Δ) were also determined in deuterated methanol by direct detection of the emission of $^1O_2$ at 1270 nm. Φ_Δ values lower than 0.04 were found for all complexes with the exception of [**3**]PF_6, which produced $^1O_2$ with a photoefficiency (Φ_Δ) of 0.11. Interestingly, $[Ru(phbpy)(dppn)(dmso\text{-}\kappa S)]^+$ did not show any singlet oxygen production, whereas its non-cyclometalated analogue $[Ru(tpy)(dppn)(CD_3OD)]^{2+}$ and $[Ru(tpy)(dppn)(py)]^{2+}$ both have been demonstrated to be excellent PDT photosensitizers.[19]

Table 5.3. Lowest-energy absorption maxima (λ_{max}), molar absorption coefficients at λ_{max} (ε in M^{-1} x cm^{-1}), photosubstitution quantum yields (Φ_{450}) at 298 K, $^1O_2$ quantum yields (Φ_Δ) at 293 K and phosphorescence quantum yield (Φ_P) for [**1**]PF_6 – [**11**]PF_6.

Complex		λ_{max} ($\varepsilon_{max\ in\ M^{-1}\ cm^{-1}}$)[a]	λ_{em} (nm)	Φ_Δ[b]	Φ_P[b]
[**1**]PF_6	$[Ru(phbpy)(bpy)(dmso\text{-}\kappa S)]PF_6$	476 ($50{\cdot}10^2$)	786	$3.2{\cdot}10^{-2}$	$1.6{\cdot}10^{-4}$
[**2**]PF_6	$[Ru(phbpy)(phen)(dmso\text{-}\kappa S)]PF_6$	450 ($57{\cdot}10^{2)}$	800	$3.9{\cdot}10^{-2}$	$2.1{\cdot}10^{-4}$
[**3**]PF_6	$[Ru(phbpy)(dpq)(dmso\text{-}\kappa S)]PF_6$	451 ($83{\cdot}10^{2)}$	787	$1.1{\cdot}10^{-1}$	$2.1{\cdot}10^{-4}$
[**4**]PF_6	$[Ru(phbpy)(dppz)(dmso\text{-}\kappa S)]PF_6$	450 ($84{\cdot}10^2$)	618	$7.0{\cdot}10^{-3}$	$2.6{\cdot}10^{-4}$
[**5**]PF_6	$[Ru(phbpy)(dppn)(dmso\text{-}\kappa S)]PF_6$	450 ($75{\cdot}10^2$)	672	-	$8.4{\cdot}10^{-5}$
[**6**]PF_6	$[Ru(phbpy)(bpy)(CD_3CN)]PF_6$	525 ($71{\cdot}10^2$)			
[**7**]PF_6	$[Ru(phbpy)(phen)(CD_3CN)]PF_6$	503 ($63{\cdot}10^2$)			
[**8**]PF_6	$[Ru(phbpy)(dpq)(CD_3CN)]PF_6$	495 ($119{\cdot}10^2$)			
[**9**]PF_6	$[Ru(tpy)(bpy)(dmso\text{-}\kappa S)](PF_6)_2$	411 ($75{\cdot}10^2$)			
[**10**]PF_6	$[Ru(tpy)(bpy)(MeCN)](PF_6)_2$	455 ($91{\cdot}10^2$)			

[a] In MeCN. [b] in CD_3OD.

5.2.4 Photochemistry

Due to the exceptional thermal inertness of complexes [**1**]PF_6 – [**5**]PF_6 we attempted to substitute the dmso ligands using visible light irradiation while reactions were monitored with ^1H NMR. When a sample of [**1**]PF_6 was irradiated in acetonitrile with the white light ($h\nu \geq 410$ nm, Scheme 5.3) of a 1000 W Xenon Arc lamp fitted with a 400 nm cutoff filter, a photoproduct was formed which was later confirmed to be the acetonitrile adduct *(see below)*. As shown in Figure 5.4, the ^1H NMR spectra clearly demonstrate the formation of a single species with a doublet appearing at 9.88 ppm and a doublet disappearing at 10.49 ppm. This photochemical behavior is very similar to the photosubstitution of $[Ru(tpy)(N\text{-}N)(X)]^{2+}$, where the monodentate ligand is replaced by a solvent molecule.[20] In a similar fashion the dmso ligand in [**2**]PF_6 and [**3**]PF_6 could also be substituted with acetonitrile. However, [**4**]PF_6 and [**5**]PF_6 were not able to exchange their ligand. This is odd, given that their non-cyclometalated analogons [Ru(tpy)(dppz)(SRR')] and [Ru(tpy)(dppn)(SRR')] (SRR' = 2-(2-(2-(methylthio)ethoxy)ethoxy)ethyl-β-D-glucopyranoside) described in Chapter 3 both have been demonstrated to be photo-active.

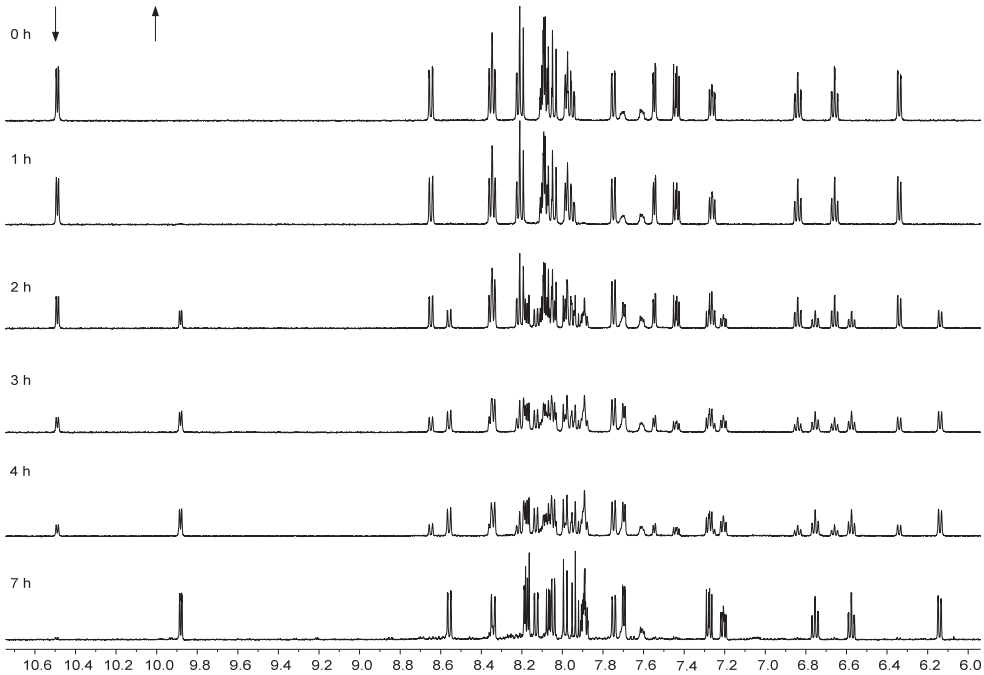

Figure 5.4 Evolution of the ^{1}H NMR spectra of **[2]**PF_6 in CD_3CN (3.0 mg in 0.6 mL) upon irradiation with white light (>410 nm) from a 1000 W Xenon Arc lamp fitted with 400 nm cutoff filter 1 cm from the light source at T = 298 K. Spectra were taken every 1 h, with t_{irr} = 7 h.

To further investigate the ability of complexes [**1**]PF_6 – [**5**]PF_6 to exchange their monodentate ligand for a solvent molecule we studied them more thoroughly using UV-vis spectroscopy (Figure 5.5). Both [**4**]PF_6 and [**5**]PF_6 were confirmed to be photochemically inert, while complex [**1**]PF_6 – [**3**]PF_6 were all found to convert to their acetonitrile counterparts with clear isosbestic points for [**1**]PF_6 (441 and 490 nm), [**2**]PF_6 (470 nm) and [**3**]PF_6 (455 nm), confirming the formation of a single species for each photoconversion. After each reaction, ESI-MS spectra were taken to confirm the formation of the acetonitrile photoproduct. The photosubstitution quantum yields (Φ_{450}) for the complexes were found to be 4.1 x 10^{-5} for [**1**]PF_6, 1.3 x 10^{-5} for [**2**]PF_6 and 2.2 x 10^{-5} for [**3**]PF_6. These values are a thousand-fold lower than those determined for $[Ru(tpy)(bpy)(dmso\text{-}\kappa S)]^{2+}$($\Phi_{450}$ = 1.6 x 10^{-2}). This is most likely caused due to the destabilization of the ^{3}MC state due to the increased electron density at the metal center brought by the strong σ-donor C-atom, and stabilization of the ^{3}MLCT, which leads to a larger energy gap between the ^{3}MLCT and ^{3}MC state and makes thermal population of the latter rather unlikely.[17] This interpretation is supported by previous work of the group of Turro, who have demonstrated that the efficiency of the photosubstitution in sterically congested cyclometalated complexes are much lower or absent, compared to their polypyridyl analogues.[12, 16] Overall, the modest but very selective photosubstitution

properties of [**1**]PF_6 - [**3**]PF_6 open new doors towards the synthesis of photo-active, chiral cyclometalated complexes.

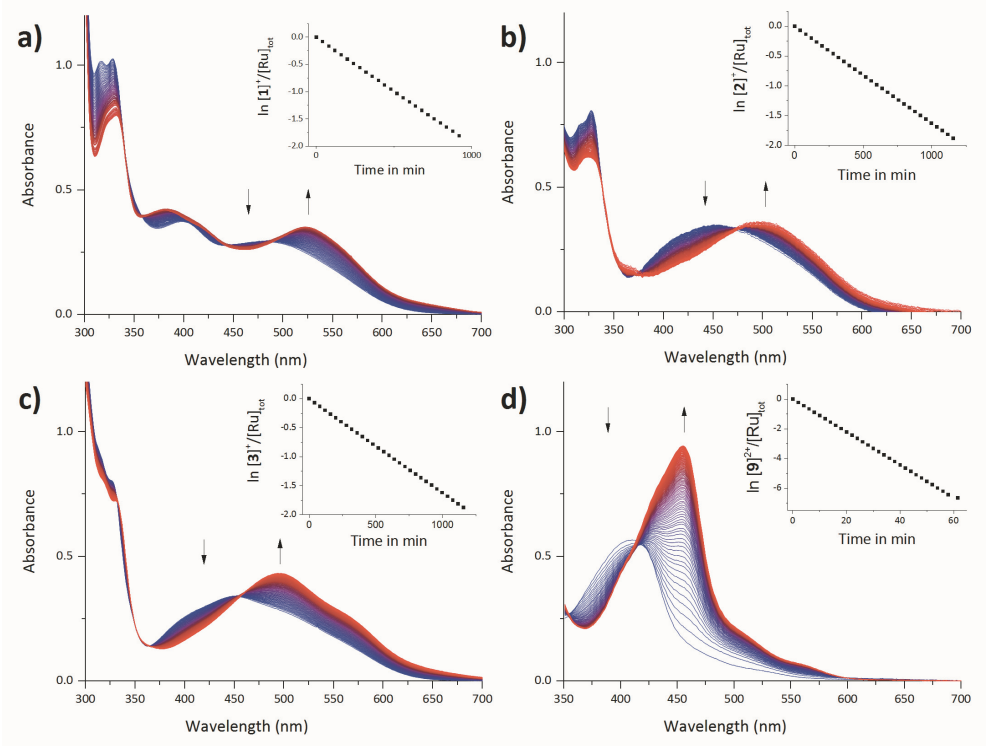

Figure 5.5 Electronic absorption spectra of [**1**]PF_6 – [**3**]PF_6 and [**9**]$(PF_6)_2$ in deoxygenated MeCN upon irradiation at 450 nm at T = 298 K. Spectra measured every 30 min (every 0.5 min for [**9**]PF_6). a). [**1**]$(PF_6)_2$ t_{irr} = 16 h, $[Ru]_{tot}$ = 5.78 x 10^{-5} M, photon flux = 1.68 x 10^{-7} mol s^{-1} . b). [**2**]$(PF_6)_2$, t_{irr} = 23 h, $[Ru]_{tot}$ =6.08 x 10^{-5} M, photon flux = 1.67 x 10^{-7} mol s^{-1}. c). [**3**]PF_6, t_{irr} = 16 h, $[Ru]_{tot}$ = 4.06 x 10^{-5} M, photon flux = 1.68 x 10^{-7} mol s^{-1}. d). [**9**]$(PF_6)_2$, t_{irr} = 1 h, $[Ru]_{tot}$ = 6.52 x 10^{-5} M, photon flux = 5.54 x 10^{-8} mol s^{-1}.

5.2.5 Electrochemistry and DFT

The electrochemical properties of complexes [**1**]PF_6 – [**9**]PF_6 were determined with cyclic voltammetry (Figure 5.6 and Table 5.4) to provide insight in the frontier orbitals of the complexes.[21] As summarized in Table 5.4, the cyclometalated dmso complexes [**1**]PF_6 – [**5**]PF_6 show semi-reversible oxidation processes (I_{pa}/I_{pc} ≈ 1) with Ru^{II}/Ru^{III} couples near ~0.30 V vs. $Fc^{0/+}$ whereas its non-cyclometalated analogon [**9**]$(PF_6)_2$ showed an irreversible $Ru^{II} \rightarrow Ru^{III}$ oxidation at 1.23 V vs. $Fc^{0/+}$. This indicates that the HOMO of the cyclometalated complexes is destabilized due to the π-donating instead of π-accepting character from the $phbpy^-$ ligand. The irreversible oxidation for [**9**]$(PF_6)_2$ is attributed to linkage isomerization of DMSO from being *S* bound to *O*-bound to the ruthenium center,[22] indicating that cyclometalation prevents redox-induced linkage isomerization, due to the increased electron density on ruthenium. When acetonitrile complex [**10**]PF_6 was used for comparison with the cyclometalated complexes instead, a similar destabilization on the HOMO energy levels was found. For the dmso complexes [**1**]PF_6 - [**5**]PF_6 the HOMO appeared at a higher potential (0.30 V *vs.* $Fc^{0/+}$) than for acetonitrile compounds [**6**]PF_6 -

[**7**]PF_6 (0.00 V *vs.* $Fc^{0/+}$) which can be explained by the origin of the monodentate ligand; *S*-dmso is a stronger π-acceptor than CD_3CN and therefore has a stronger electron withdrawing effect on ruthenium(II), which in turn leads to stabilization of the HOMO.[23] The LUMO for [**1**]PF_6 – [**3**]PF_6 was found to have very similar energy, with quasi-reversible reductions around -2.0 V *vs.* $Fc^{0/+}$, suggesting that these are phbpy-based. For [**4**]PF_6 and [**5**]PF_6 the LUMO appears to be lower in energy (-1.4 V *vs.* $Fc^{0/+}$ for [**4**]PF_6 and -1.2 V *vs.* $Fc^{0/+}$ for [**5**]PF_6) due to the strong electron-accepting properties of the dipyridophenazine moieties.[24]

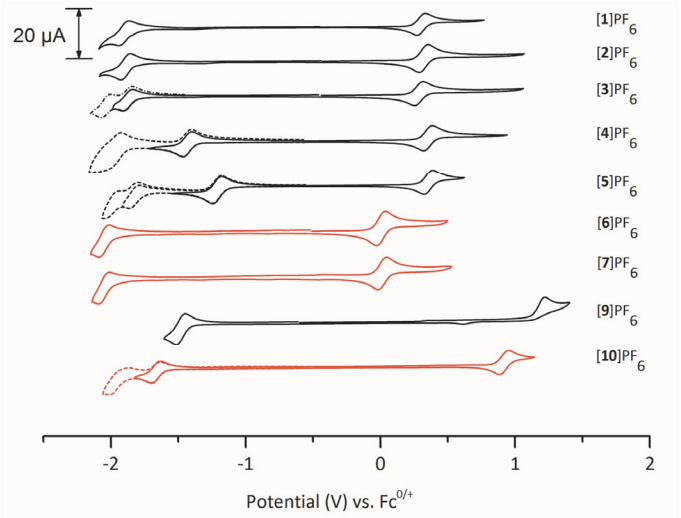

Figure 5.6 Cyclic voltammograms of cyclometalated complexes [**1**]PF_6 – [**7**]PF_6 and non-cyclometalated complexes [**9**]$(PF_6)_2$ and [**10**]$(PF_6)_2$. Scan rate 100 mV s^{-1}, with the exception of [**4**]PF_6, [**6**]PF_6, [**7**]PF_6 and [**9**]PF_6 which were measured at 200 mV s^{-1}. L = dmso-κS or CD_3CN.

Table 5.4. Redox potentials measured with cyclic voltammetry (vs Fc^0/Fc^+) in MeCN with $[Bu_4N]PF_6$ as supporting electrolyte. Complexes were measured at 298 K with a scan rate of 100 mV.s^{-1}, with the exception of [**4**]PF_6, [6]PF_6 [**7**]PF_6 and [**8**]PF_6 which were measured at 200 mV.s^{-1}.

		$E_{1/2}$ (V)	i_{pa}/i_{pc}	$E_{1/2}$ (V)	i_{pc}/i_{pa}
[Ru(phbpy)(bpy)(dmso-κS)]PF_6	[**1**]PF_6	+0.30	0.99	-1.90	1.47
[Ru(phbpy)(phen)(dmso-κS)]PF_6	[**2**]PF_6	+0.32	1.02	-1.89	1.11
[Ru(phbpy)(dpq)(dmso-κS)]PF_6	[**3**]PF_6	+0.29	1.01	-1.87, -1.95	0.66, 2.23
[Ru(phbpy)(dppz)(dmso-κS)]PF_6	[**4**]PF_6	+0.35	1.04	-1.43, -2.00	1.03, -
[Ru(phbpy)(dppn)(dmso-κS)]PF_6	[**5**]PF_6	+0.36	1.05	-1.21, -1.82, -2.01	1.07, 1.52
[Ru(phbpy)(bpy)(CD_3CN)]PF_6	[**6**]PF_6	0.00	1.00	-2.05	1.34
[Ru(phbpy)(phen)(CD_3CN)]PF_6	[**7**]PF_6	+0.02	1.04	-2.05	-1.38
[Ru(tpy)(bpy)(DMSO)]$(PF_6)_2$	[**9**]$(PF_6)_2$	+1.23[a]	-	-1.48	1.00
[Ru(tpy)(bpy)(MeCN)]$(PF_6)_2$	[**10**]$(PF_6)_2$	+0.92	0.95	-1.67	1.06

[a] E_{pa}

To provide further insight on the frontier orbitals of these complexes, their HOMO – LUMO gap was plotted in an energy diagram (Figure 5.7, left). This plot revealed that the HOMO-LUMO gap between complexes [**1**]PF_6 – [**3**]PF_6 is very similar, with ΔE (ΔE_{pa}-E_{pc}) ~ 2.2 V *vs.* $Fc^{0/+}$. This value is significantly lower than that of the tpy analogues $[Ru(tpy)(bpy)(L)]^{2+}$ with L = S-dmso and MeCN (ΔE = 2.6 and 2.7 V *vs.* $Fc^{0/+}$), which is

explained by an increase of the energy of the HOMO due to the π-donating properties of the phbpy$^-$ ligand.[16] Surprisingly, for [**4**]PF_6 and [**5**]PF_6 however, the ΔE values found (ΔE -1.6 V for [**4**]PF_6 and ΔE 1.8 V for [**5**]PF_6) are much lower than those found for complexes [**1**]PF_6 – [**3**]PF_6, suggesting that the dppz and dppn ligands have a stabilizing effect on the ^{1}MLCT level.

To further elaborate that hypothesis, we then performed density functional theory (DFT) calculations at the BPE0/TZP level using the conductor-like screening model (COSMO) to simulate solvent effects. The calculated HOMO and LUMO energy levels show a trend (Figure 5.7, right), that fitted very well with the results acquired from cyclic voltammetry. Furthermore, these calculations revealed that for complex [**3**]$^+$, [**4**]$^+$ and [**5**]$^+$ the LUMO is located on the bidentate ligand dpq, dppz, and dppn, respectively (Figure S.IV.3-5), whereas for [**1**]PF_6 and [**2**]PF_6 it is located on the phbpy$^-$ ligand. Like for [Ru(tpy)(dppz)(L)]$^{2+}$, for which the LUMO was also found on the dppz ligand,[24] for complexes [**4**]PF_6 and [**5**]PF_6 extending the conjugation of the bidentate ligand results in a shift of the LUMO from the tridentate to the bidentate ligand. For the more conjugated complexes [**4**]PF_6 and [**5**]PF_6 this does not affect the main ^{1}MLCT band (Figure 3). However, assuming that the photochemistry occurs from the lowest excited ^{1}MLCT, this would lead to a ^{3}MLCT state for [**4**]PF_6 and [**5**]PF_6 too low in energy to allow thermal population of ^{3}MC state. Therefore making alternative pathways, such as non-radiative decay a preferred pathway over photo-dissociation.[25]

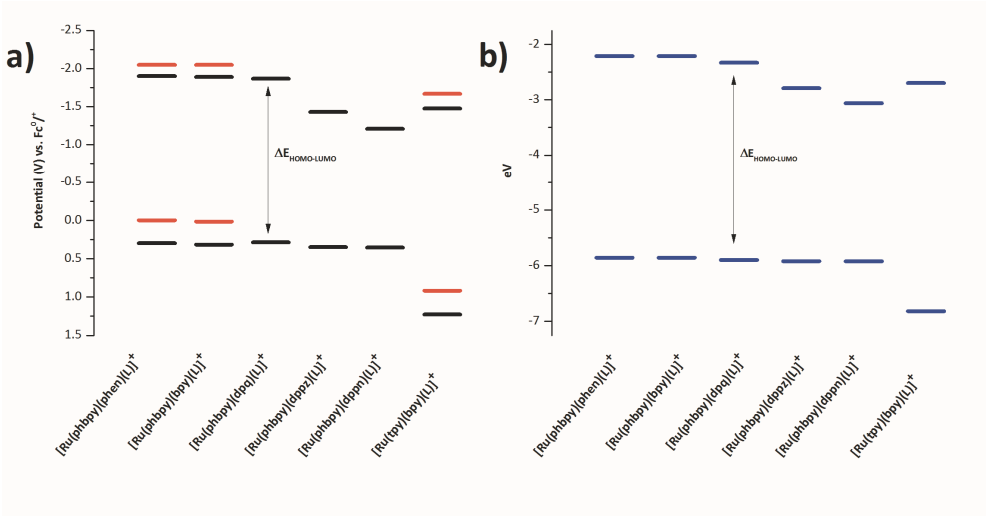

Figure 5.7 a). HOMO and LUMO orbital energy diagram derived from cyclic voltammetry data for complexes with general formula [Ru(phenbpy)(N-N)L]+ with N-N = phen, bpy, dpq, dppz and dppn or [Ru(tpy)(bpy)L]$^+$. **Red** lines L = S-dmso. **Black** lines L = MeCN/CD_3CN. **b).** HOMO and LUMO orbital energy diagram derived from DFT calculations, L = dmso-κS.

5.2.6 Resolving diastereomers

The photochemical lability of the complexes [**1**]PF_6 – [**3**]PF_6 allowed us to investigate whether separation of their respected enantiomers was possible. Similar to the approach

described in the previous section (§ 5.2.4), compound [**2**]PF_6 was converted to photoproduct [**7**]PF_6 using white light in deuterated acetonitrile, which allowed the reaction to be monitored with ^{1}H NMR spectroscopy. After completion of the reaction (~7 h) an attempt was made to resolve this intermediate [**7**]PF_6 with either a chiral HPLC column or by crystallization using sodium (*+*)-tartrate, however without success. An alternative procedure was therefore used: [**7**]PF_6 was allowed to react with an excess of enantiomerically pure (*R*)-methyl *p*-tolylsulfoxide in MeOH, affording a (1:1) mixture of diastereomers of (anticlockwise/clockwise) A/C-[Ru(phbpy)(phen)(*R*)-Methyl *p*-tolylsulfoxide)]PF_6, [**11-A/C**]PF_6 (Scheme 5.3). Subsequent purification over a chiral HPLC column, afforded [**11-A**]PF_6 and [**11-C**]PF_6 as their respective diastereomers in 9% yield (6% over two steps for [**11-A**]PF_6 and 3% over two steps for [**11-C**]PF_6 (Figure S.IV.6).

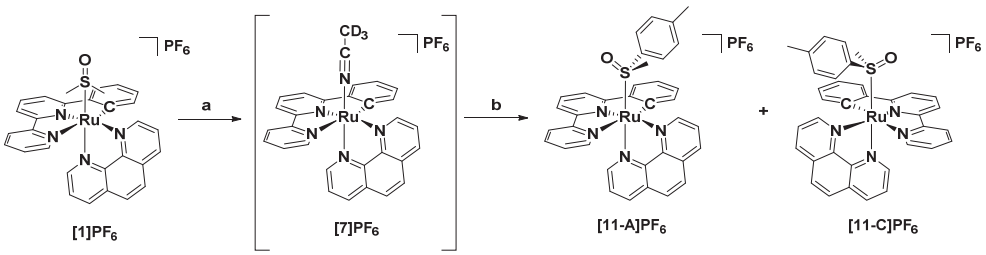

Scheme 5.3. Reagents and conditions for the synthesis of [**11-A/C**]PF_6. a). hv, ≥ 410 nm. b). (R)-Methyl *p*-tolylsulfoxide in MeOH, reflux, 16 h. (6% over two steps for [**10-*A***]PF_6, 3% over two steps for [**10-*C***]PF_6).

^{1}H NMR confirmed that fraction 1 corresponded to the R-C diastereomer, which is most apparent because of its more shielded α-proton of phen appearing at 10.64 ppm (Figure 5.8). Fraction 2 contained the R-A diastereomer, with a doublet appearing at 10.74 ppm (Figure 8). This deshielding effect on the α-proton on phen is most likely attributed to the interaction of the tolyl group with the bidentate ligand, which is supported by NOESY experiments (Figure S.IV.6), which show the absence of interaction between the methyl of the sulfoxide and phen, whereas this interaction is weakly observed for [**11-A**]PF_6 (Figure S.IV.7). However, crystal structures are needed to confirm the stereochemistry of these complexes.

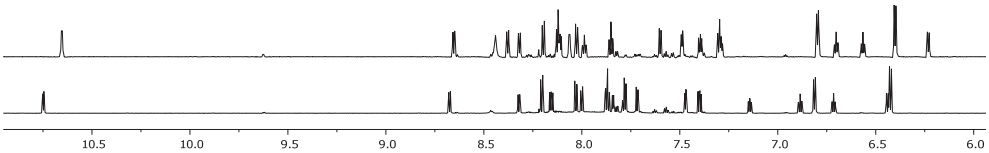

Figure 5.8. ^{1}HNMR spectrum (850 Mhz) of [**11-C**]PF_6 (top) and [**11-A**]PF_6 (bottom).

Since both complexes [**11-A**]PF_6 and [**11-C**]PF_6 were isolated as diastereomers and were not resolved as their respective enantiomers [**7-A**]PF_6 and [**7-C**]PF_6, determining their specific rotation would not provide any useful information about their chirality. Circular dichroism (CD) was used instead. The CD spectra (Figure 5.9) displayed symmetrical curves

typical for enantiomers, except in the region below 250 nm where the contribution of the chiral (*R*)-tolylsulfoxide becomes non-negligible.[26] At higher wavelengths (260 – 600 nm), either positive or negative Cotton effects were observed for [**11-A**]PF_6 or [**11-C**]PF_6 complex, which are most likely only originating from metal-based transitions. Theoretically, resolution of these complexes by performing blue light irradiation in acetonitrile may be tempting. However, photosubstitution is usually accompanied by racemization of the coordination sphere, so that thermal ligand substitution would be preferred.[27] The exceptional thermal stability of the sulfoxide cyclometalated complexes prevented us from obtaining isolated enantiomers. However, CD of the diastereoisomers [**11-A**]PF_6 and [**11-C**]PF_6 provided a clear proof of the chirality of these complexes.

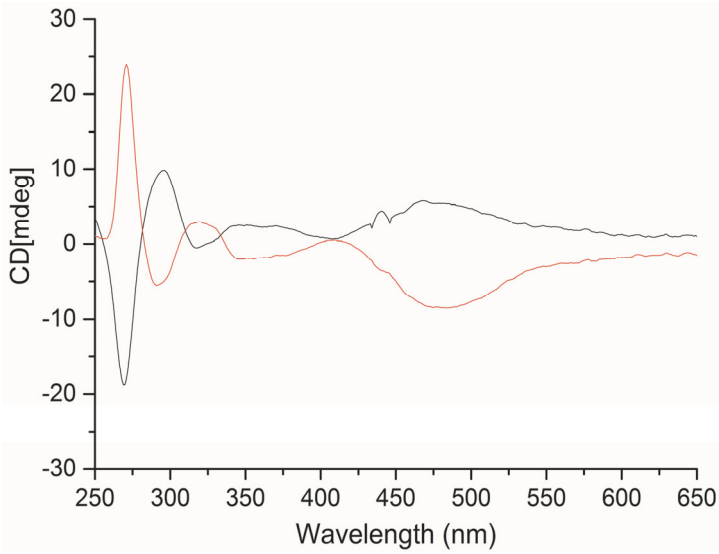

Figure 5.9. Superposition of CD spectra of first fraction ([**11-C**]PF_6) and second fraction ([**11-A**]PF_6) eluted diastereoisomers. T = 293 K, *c* = 5 x 10^{-5} M in MeCN.

5.2.7 DNA interaction and cytotoxicity

The cytotoxic properties of [**1**]PF_6 – [**3**]PF_6 were investigated in the dark as well under green light irradiation (λ = 520nm, 10 min, 25.0 ± 1.9 mW, 15 ± 1.1 J cm^{-2}) against two different human cancer cell lines, A549 (lung cancer) and MCF-7 (breast cancer). Considering the poor photosensitizing and photodissociation properties of [**4**]PF_6 and [**5**]PF_6, these complexes were only tested in the dark after a high-throughput screening confirmed that there are no differences in EC_{50} for these complexes before and after light irradiation. Cells were seeded, treated with a concentration series of **[1]**PF_6 – **[5]**PF_6 at t = 24 h, irradiated or maintained in the dark after media refreshment (t = 48 h), followed by cell viability determination at t = 96 h using the sulforhodamine B (SRB) assay.[28] The cell-growth inhibition concentrations (EC_{50}) are reported in Table 5.5. In the dark complexes

[**1**]PF_6 – [**3**]PF_6 are moderately to non-cytotoxic with EC_{50} values between 43 and >100 μM. However, upon green light irradiation complex [**1**]PF_6 and [**3**]PF_6 showed an increase in cytotoxicity resulting in photo-indices ranging from 1.4 to 9.3 reaching low micromolar (<10 μM) cytotoxicity values. This effect might be ascribed to the generation of reactive oxygen species since these three complexes have been demonstrated to be poor to moderate singlet oxygen sensitizers (Φ_Δ = 0.032 - 0.11). However, as shown in Figure S.IV.8, our DNA studies in the presence of green light did not show the formation of any DNA adducts or open circular DNA, which suggests that these compounds have another target than nuclear DNA. This result is in contrast to that of reported analogues, such as the D-glucose conjugated $[Ru(tpy)(dppn)(SRR')]^{2+}$ complex reported in chapter 3, which was demonstrated to have a very high affinity for (mitochondrial) DNA in the dark and cleaved DNA.[19a] On the other hand, complexes [**4**]PF_6 and [**5**]PF_6 were demonstrated to be very cytotoxic to both cell lines, approaching EC_{50} values in the low micromolar to sub-micromolar range against both A549 and MCF-7 cells. This result is in accordance with other cyclometalated complexes reported by Fetzer et. al. who have shown that more lipophilic cyclometalated complexes often have an increased cycotoxic effect on cancer cells, compared to polypyridyl analogues.[29] However, even for [**4**]PF_6 and [**5**]PF_6 complexes, which contain the well-known intercalators dppz and dppn,[3, 19a, 30] no DNA interaction was observed, even at high MC:BP ratios of 5:1, therefore suggesting an alternative mode of action, such as disturbance of oxido-reductase enzymes.[29]

Table 5.5. (Photo)cytotoxicity for [**1**]PF_6 - [**5**]PF_6 expressed as effective concentrations (EC_{50} in μM) in the dark and after irradiation with green light (520 ± 38 nm, 25.0 mW ± 1.9 · cm^{-2}, 10 minutes, 15 · J cm^{-2} ± 1.14) in A549 and MCF-7 cells. Values are reported in μM with ±95% confidence intervals (CI). Photocytotoxicity index (PI = $EC_{50,dark}/EC_{50,520\ nm}$).

		A549			MCF-7		
Complex	Light dose (J cm^{-2})	EC_{50} (μM)	±CI (95%)	PI	EC_{50} (μM)	±CI (95%)	PI
[**1**]PF_6	0	>100	-	>1.4	67	+14 -10	
	15	69	+6.8 -6.1		21	+5.5 -4.2	
[**2**]PF_6	0	43	+13 -9.5	5.7	18	+3.9 -3.2	5.8
	15	7.6	+2.0 -1.7		3.1	+0.49 -0.44	
[**3**]PF_6	0	62	+20 -14	9.3	11	+3.6 -2.8	5.5
	15	6.7	+1.5 -1.2		2.0	+0.72 -0.56	
[**4**]PF_6	0	2.6	+0.37 -0.32	-	1.5	+0.28 -0.24	-
	15	n.d.	-	-	n.d.	-	-
[**5**]PF_6	0	1.2	+0.17 -0.14	-	0.51	+0.059 -0.055	-
	15	n.d.	-	-	n.d.	-	-

5.3 Discussion

Three of the presented cycloruthenated complexes ([**1**]PF_6 – [**3**]PF_6) have been demonstrated to have photodissociative properties in the presence of acetonitrile. Recent examples of the group of Turro have shown that complexes such as *cis*-[Ru(phpy)(phen)$(CH_3CN)_2$]PF_6 are as photoactive as their non-cyclometalated counterparts, with a reported photosubstitution quantum yield (Φ_P) of 0.25.[12] However, this value was obtained by irradiation in dichloromethane in the presence of 2 mM tetrabutyl ammonium chloride. It has been a well-established fact that more polar solvents have a stabilizing effect on ^{3}MLCT states, without affecting the ^{3}MC states, thereby increasing the ^{3}MC-^{3}MLCT energy gap. Therefore providing an explanation for the high photosubstitution quantum yield for [Ru(phpy)(phen)$(CH_3CN)_2$]PF_6 in dichloromethane. A more recent report by Albani et. al. has shown that for [Ru$(biq)_2$(phpy)]PF_6 the $phpy^-$ ligand increases the energy of the ^{3}MC state, which in their case completely prevents photodissociation.[16] Our findings show that the ligand exchange efficiency upon irradiation of complexes [**1**]PF_6 – [**5**]PF_6 is mostly determined by the cyclometalated ligand, which seems to have a great effect on the energy of both the HOMO and LUMO. However, when phenazine based ligands are introduced in the [Ru(phbpy)(N-N)(dmso-κS)]$^+$ scaffold, the LUMO is shifted from the tridentate ligand to the bidentate ligand. This has multiple consequences. First, [**3**]PF_6 both generates modest amounts of $^1O_2$ (Φ_Δ = 0.11) due to competition with a $^3\pi\pi^*$ state and is able to substitute its monodentate ligand with a solvent molecule. Second, the photo-reactivity of these complexes seems to be diminished due to the stabilized ^{1}MLCT state, which makes population of the ^{3}MC from the lowered ^{3}MLCT state very unlikely for both complex [**4**]PF_6 and [**5**]PF_6. This effect is in great contrast to the photochemical behavior of the non-cyclometalated compounds, which undergo efficient photosubstitution. For example, compared to [**4**]PF_6, [Ru(tpy)(dppz)(SRR')]$^{2+}$ -reported in chapter 4- has a photosubstitution quantum yield of ~0.02, whereas [Ru(tpy)(dppn)(SRR')]$^{2+}$ is able to exchange its monodentate ligand upon light irradiation and a good $^1O_2$ sensitizer (Φ_Δ = 0.71).[19a] Therefore demonstrating that modifications on the bidentate ligand in the [Ru(phbpy)(N-N)(dmso-κS)]$^+$ scaffold have a major effect on its photo-reactivity.

5.4 Conclusion

In this work we have presented five new cycloruthenated complexes ([**1**]PF_6 – [**5**]PF_6) based on the [Ru(phbpy)(N-N)(L)]$^+$ architecture. We have demonstrated the exceptional thermal stability of these complexes towards thermal substitution, and provided a thorough description of their photophysical behavior. In spite of their low $^1O_2$ generation quantum yields, complexes [**1**]PF_6 - [**3**]PF_6 were found to be photocytotoxic, while [**4**]PF_6 and [**5**]PF_6 were not photocytotoxicity but very cytotoxic in the dark. The submicromolar

EC_{50} values found for these complexes provide an incentive to study them in more detail, since they have an unexpected poor binding affinity for DNA. Finally, we have demonstrated that we can synthesize and separate a set of specific diastereomers (**[11-A]**PF_6 and **[11-C]**PF_6) from [**2**]PF_6 using a two-step photochemical and thermal approach. To conclude, these results open interesting new prospects in the field of photo-active chiral anticancer drugs.

5.5 Experimental

5.5.1 General

Reagents were purchased from Sigma-Aldrich and used without further purification. Dpq,[31] dppz,[31] dppn,[32] Hphbpy,[33] (*R*)-(+)-methyl *p*-tolyl sulfoxide[34] and *cis*-$Ru(dmso)_4Cl_2$[35] were synthesized according to reported procedures. Dry solvents were collected from a Pure Solve MD5 solvent dispenser from Demaco Holland BV. For all inorganic reactions solvents were deoxygenated by bubbling argon through the solution for 30 minutes and carried out under an inert atmosphere in the dark, unless stated otherwise. Solvents were removed under vacuum with a rotary evaporator in the dark at 30 °C, unless stated otherwise. Flash chromatography was performed on silica gel (Screening devices B.V.) with a particle size of 40 - 64 µM and a pore size of 60 Å. Chiral HPLC was performed on a Jupiter® 4µm Proteo 90 Å 3000 UHPLC (250 x 21.2 mm, flow rate 14 $mL \cdot min^{-1}$). TLC analysis was conducted on TLC aluminium foils with silica gel matrix (Supelco, silica gel 60, 56524) with detection by UV-absorption (254 nm). NMR spectra were recorded on a Bruker AV-400 or AV-500. ^1H NMR and ^{13}C NMR spectra were recorded in [D_6]acetone, [D_3]acetonitrile and [D_6]DMSO with chemical shifts (δ) relative to the solvent peak. High resolution mass spectra were recorded by direct injection (2 µl of 2 µM solution in water/acetonitrile; 50/50; v/v and 0.1% formic acid) in a mass spectrometer (Thermo Finnigan LTQ Orbitrap) equipped with an electrospray ion source in positive mode (source voltage 3.5 kV, sheath gas flow 10, capillary temperature 250 °C) with resolution R = 60000 at m/z 400 (mass range m/z = 150 – 2000) and dioctylphtalate (m/z = 391.28428) as a lock mass. The high-resolution mass spectrometer was calibrated prior to measurements with a calibration mixture (Thermo Finnigan).

5.5.2 Synthesis

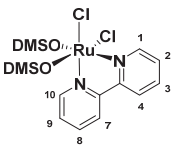

[Ru(bpy)(dmso)$_2$Cl$_2$], [**12**]: *cis*-[$Ru(dmso)_4Cl_2$] (200 mg, 0.410 mmol) and bpy (64.0 mg, 0.410 mmol) were dissolved in deoxygenated EtOH/DMSO (3.2 mL, 16:1) and heated at reflux for 2 h. After cooling to rt, the resulting precipitate was filtered, washed with cold ethanol (5 mL), diethyl ether (15 mL) and dried *in vacuo* affording the title compound as an orange powder (168 mg, 0.350 mmol, 86%). ^1H NMR (400 MHz,

[D_6]DMSO) δ = 9.66 (d, *J* = 4.5 Hz, 1H, 1), 9.55 (d, *J* = 4.5 Hz, 1H, 10), 8.66 (d, *J* = 8.1 Hz, 1H, 7), 8.61 (d, *J* = 8.2 Hz, 1H, 4), 8.22 (td, *J* = 7.8, 1.6 Hz, 1H, 8), 8.10 (td, *J* = 7.8, 1.5 Hz, 1H, 3), 7.77 (dd, *J* = 7.2, 5.6 Hz, 1H, 9), 7.61 (dd, *J* = 7.4, 5.7 Hz, 1H, 2), 3.40 (s, 3H, CH_3), 3.36 (s, 3H, CH_3), 2.98 (s, 3H, CH_3), 2.28 (s, 3H, CH_3); HRMS: m/z calcd for $[C_{14}H_{20}Cl_2N_2O_2RuS_2 - Cl]^+$: 448.96982; found: 489.96900; elemental analysis calcd (%) for [**12**]: C 34.71, H 4.16, N 5.78; found: C 34.82, H 4.31, N 5.53.

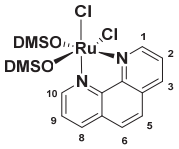

[Ru(phen)(dmso)$_2$Cl$_2$], [**13**]: The procedure described for [**12**] was followed using [*cis*-Ru(dmso)$_4$Cl$_2$] (100 mg, 0.210 mmol) and phen (38.0 mg, 0.210 mmol) yielding the product as an orange powder (82.0 mg, 0.160 mmol, 77%). ^{1}H NMR (400 MHz, [D_6]DMSO) δ = 9.96 (d, *J* = 5.4 Hz, 1H, 1), 9.83 (d, *J* = 5.2 Hz, 10), 8.87 (d, *J* = 8.2 Hz, 1H, 8), 8.74 (d, *J* = 8.3 Hz, 3), 8.34 – 8.22 (m, 2H, 5, 6), 8.17 (dd, 1H, *J* = 8.2, 5.4 Hz, 9), 8.01 (dd, *J* = 8.2, 5.4 Hz, 1H, 2), 3.48 (s, 3H, CH_3), 3.43 (s, 3H, CH_3), 2.94 (s, 3H, CH_3), 2.15 (s, 3H, CH_3); HRMS: m/z calcd for $[C_{16}H_{20}Cl_2N_2O_2RuS_2 - Cl]^+$: 472.96962; found: 472.96904; elemental analysis calcd (%) for [**13**]: C 37.80, H 3.97, N 5.51; found: C 37.64, H 4.03, N 5.58.

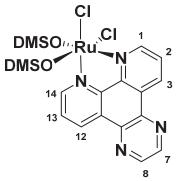

[Ru(dpq)(dmso)$_2$Cl$_2$], [**14**]: The procedure described for [**12**] was followed using *cis*-Ru(dmso)$_4$Cl$_2$ (200 mg, 0.410 mmol) and dpq (95.0 mg, 0.410 mmol) yielding the product as an orange brown powder (220 mg, 0.390 mmol, 95%). ^{1}H NMR (400 MHz, [D_6]DMSO) δ = 10.13 (d, *J* = 5.5 Hz, 1H, 1), 10.00 (d, *J* = 6.5 Hz, 1H, 14), 9.66 (d, *J* = 6.9 Hz, 1H, 12), 9.53 (d, *J* = 8.2 Hz, 1H, 3), 9.35 (m, 2H, 7, 8), 8.33 (dd, *J* = 8.2, 5.3 Hz, 1H, 13), 8.17 (dd, *J* = 8.2, 5.5 Hz, 1H, 2), 3.50 (s, 3H, CH_3), 3.45 (s, 3H, CH_3), 2.95 (s, 3H, CH_3), 2.28 (s, 3H, CH_3); HRMS: m/z calcd for $[C_{18}H_{20}Cl_2N_4O_2RuS_2 - Cl]^+$: 524.975969; found: 524.97535; elemental analysis calcd (%) for [**14**]: C 38.57, H 3.60, N 10.00 ; C 37.73; found: H 4.12, N 9.50.

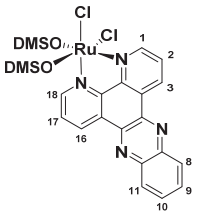

[Ru(dppz)(dmso)$_2$Cl$_2$], [**15**]: [*cis*-[Ru(dmso)$_4$Cl$_2$] (100 mg, 0.210 mmol) and dppz (60.0 mg, 0.210 mmol) in ethanol (3 mL) and DMSO (0.2 mL) were refluxed for 2 h. The reaction was cooled down to room temperature and the resulting precipitate was filtered, washed with cold ethanol (5 mL) and diethyl ether (15 mL). The crude was then redissolved in a minimal amount of acetone, and precipitated with Et_2O to afford the title compound as a light brown powder (110 mg, 0.18 mmol, 87%). ^{1}H NMR (400 MHz, [D_6]DMSO) δ = 10.10 (d, *J* = 4.2 Hz, 1H, 1), 9.98 (d, *J* = 3.9 Hz, 1H, 18), 9.73 (d, *J* = 8.0 Hz, 1H, 16), 9.61 (d, *J* = 7.7 Hz, 1H, 3), 8.54 – 8.46 (m, 2H, 8, 11), 8.36 – 8.29 (m, 1H, 17), 8.20 – 8.12 (m, 3H, 2, 9, 10), 3.49 (s, 3H, CH_3), 3.46 (s, 3H, CH_3), 2.95 (s, 3H, CH_3), 2.32 (s, 3H, CH_3); HRMS: m/z calcd for $[C_{22}H_{22}Cl_2N_4O_2RuS_2 - Cl]^+$:

574.99162; found: 574.99119; elemental analysis calcd (%) for [**15**].2H_2O: C 49.49, H 3.58, N 9.62; found: C 48.69, H 3.43, N 9.35.

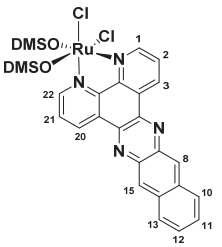

[Ru(dppn)(dmso)$_2$Cl$_2$], [**16**]: The same procedure was followed as described for [**15**] using *cis*-[Ru(dmso)$_4$Cl$_2$] (100 mg, 0.206 mmol) and dppn (70.0 mg, 0.211 mmol) to afford the product as an light brown powder (131 mg, 0.198 mmol, 96%). ^{1}H NMR (400 MHz, [D_6]DMSO) δ = 10.09 (d, *J* = 5.5 Hz, 1H, 1), 9.96 (d, *J* = 4.3 Hz, 1H, 22), 9.72 (d, *J* = 6.9 Hz, 1H, 21), 9.60 (d, *J* = 7.9 Hz, 1H, 3), 9.23 (d, *J* = 2.4 Hz, 2H, 8, 15), 8.49 – 8.39 (m, 2H, 10, 13), 8.37 – 8.27 (m, 1H, 21), 8.19 – 8.10 (m, 1H, 2), 7.85 – 7.71 (m, 2H, 11, 12), 3.50 (s, 3H, CH_3), 3.46 (s, 3H, CH_3), 2.96 (s, 3H, CH_3), 2.35 (s, 3H, CH_3); HRMS: m/z calcd for [$C_{26}H_{24}ClN_4O_2RuS_2$ – Cl]$^+$: 625.00727; found: 625.00679; elemental analysis calcd (%) for [**16**]: C 47.27, H 3.66, N 8.48; found: C 47.47, H 3.79, N 8.36.

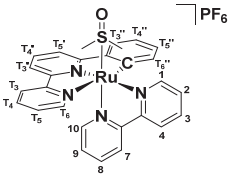

[Ru(phbpy)(bpy)(dmso)]PF$_6$, [**1**]PF_6: [Ru(bpy)(dmso)$_2$Cl$_2$] (122 mg, 0.250 mmol) and Hphbpy (58 mg 0.25 mmol) were dissolved in a mixture of MeOH/H_2O (15 mL, 5:1) and to this mixture were added 4 drops of *N*-ethylmorpholine. After heating at reflux for 16 h, solvents were removed *in vacuo,* followed by purification over silica (0 – 15% MeOH in DCM) and salt metathesis using aqueous KPF_6. The resulting precipitate was filtered and washed with water (3x) affording the title compound as a red powder (116 mg, 0.16 mmol, 65%). *Rf* = 0.30 (10% MeOH in DCM); ^{1}H NMR (400 MHz, [D_6]acetone) δ = 10.32 (d, *J* = 5.9 Hz, 1H, 1), 8.72 (d, *J* = 8.2 Hz, 1H, 4), 8.64 (d, *J* = 8.2 Hz, 1H, T_5'), 8.58 (d, *J* = 8.2 Hz, 1H, 7), 8.46 (d, *J* = 7.9 Hz, 1H, T_3'), 8.30 (d, *J* = 5.4 Hz, 1H, T_6), 8.26 – 8.10 (m, 4H, 3, T_5', T_4' T_3), 7.90 (t, *J* = 7.9 Hz, 1H, 1H, 8), 7.84 (t, *J* = 7.5 Hz, 2H, 2, T_3''), 7.59 – 7.50 (m, 1H, T_5), 7.39 (d, *J* = 5.6 Hz, 1H, 10), 7.25 (t, *J* = 6.6 Hz, 1H, 9), 6.89 (t, *J* = 7.5 Hz, 1H, T_4"), 6.81 (t, *J* = 7.3 Hz, 1H, T_5"), 6.61 (d, *J* = 7.4 Hz, 1H, T_6"), 2.41 (s, 3H, CH_3), 2.25 (s, 3H, CH_3); ^{13}C NMR (101 MHz, [D_6]acetone) δ = 181.9 (C_q), 168.4 (C_q), 157.9 (C_q), 156.8 (C_q), 156.0 (C_q), 154.9 (C_H, 1), 153.1 (C_H, T_6), 149.0 (CH, 10), 148,0 (C_q), 139.7 (C_H, T_4), 138.4 (C_H, T_6"), 138.2 (C_H, T_4'), 137.7 (C_H, 8), 136.0 (C_H, 3), 130.9 (C_H, T_5"), 128.7 (C_H, T_5), 127.3 (C_H, 9), 127.2 (C_H, 2), 126.2 (C_H, T_3"), 124.9 (C_H, T_3), 124.7 (C_H, 4), 123.8 (C_H, 7), 123.2 (C_H, T_4"), 121.1 (C_H, T_3'), 120.4 (C_H, T_5'), 45.6 (CH_3), 43.5 (CH_3); HRMS: m/z calcd for [$C_{28}H_{25}N_4ORuS$ – PF_6]: 567.07926; found: 567.07885; elemental analysis calcd (%) for [**1**]PF_6 : C 47.26, H 3.54, N 7.87; found: C 46.54, H 4.19, N 7.35.

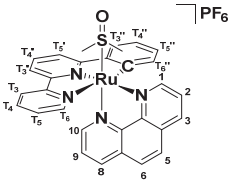

[Ru(phbpy)(phen)(dmso)]PF$_6$, [**2**]PF_6: The same procedure was followed as described for [**6**]PF_6 using [Ru(phen)(dmso)$_2$Cl$_2$] (114 mg, 0.22 mmol) and Hphbpy (51 mg, 0.22 mmol) to afford the product as a red powder (113 mg, 0.15 mmol, 68%). ^{1}H NMR (400

MHz, [D_6]acetone) δ = 10.67 (d, *J* = 5.4 Hz, 1H, 1), 8.82 (d, *J* = 8.2 Hz, 1H, 3), 8.64 (d, *J* = 8.1 Hz, 1H, T_3), 8.51 (dd, *J* = 8.2, 4.7 Hz, 2H, 8, T_5), 8.35 (d, *J* = 8.9 Hz, 1H, 5), 8.28 (d, *J* = 8.1 Hz, 1H, T_5'), 8.26 – 8.15 (m, 3H, 2, 6, T_6, T_4'), 8.11 (t, *J* = 7.9 Hz, 1H, T_4), 7.84 (d, *J* = 7.7 Hz, 1H, T_3"), 7.76 (d, *J* = 5.2 Hz, 1H, 10), 7.62 (dd, *J* = 8.3, 5.1 Hz, 1H, 9), 7.46 – 7.36 (m, 1H, T_5), 6.83 (t, *J* = 7.5 Hz, 1H, T_4"), 6.66 (t, *J* = 7.3 Hz, 1H, T_5"), 6.41 (d, *J* = 7.5 Hz, 1H, T_6"), 2.47 (s, 3H, CH_3), 2.35 (s, 3H, CH_3); ^{13}C NMR (101 MHz, [D_6]acetone) δ = 180.9 (C_q), 167.6 (C_q), 157.2 (C_q), 157.1 (C_q), 154.3 (CH, 1), 152.4 (C_H, T_4'), 148.6 (C_H, 10), 147.3 (C_q), 147.2 (C_q), 145.5 (C_q), 138.8 (C_H, T_4), 137.6 (CH, T_6"), 137.5 (C_H, T_6), 136.0 (C_H, T_5), 134.3 (C_H, 3), 131.3 (C_q), 130.2 (C_q), 129.8 (C_H, T_5"), 128.5 (C_H, 5), 127.7 (C_H, T_5), 127.4 (C_H, 6), 125.6 (C_H, 2), 125.3 (CH, T_3"), 125.0 (C_H, 9), 124.0 (C_H, T_2), 122.3 (C_H, T_4"), 120.3 (C_H, 8), 119.6 (C_H, T_5'), 44.7 (CH_3), 43.2 (CH_3). HRMS: m/z calcd for $[C_{30}H_{25}N_4ORuS - PF_6]^+$: 591.07926; found: 591.07887; elemental analysis calcd (%) for [**2**]PF_6: C 48.98, H 3.43, N 7.62; C 48.46, H 3.57, N 7.47.

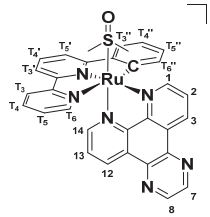

[Ru(phbpy)(dpq)(dmso)]PF_6, [**3**]PF_6: The same procedure was followed as described for [6]PF_6 using [Ru(dpq)(dmso)$_2$Cl$_2$] (115 mg, 0.210 mmol) and Hphbpy (49.0 mg, 0.220 mmol) to afford the product as a red powder (120 mg 0.150 mmol 74%). ^{1}H NMR (400 MHz, [D_6]acetone) δ = 10.80 (d, *J* = 4.3 Hz, 1H, 1), 9.66 (d, *J* = 6.9 Hz, 1H, 3), 9.32 – 9.22 (m, 2H, 7, 12), 9.16 (d, *J* = 2.1 Hz, 1H, 8), 8.64 (d, *J* = 8.2 Hz, 1H, T_3), 8.50 (d, *J* = 6.9 Hz, 1H, T_3'), 8.38 – 8.26 (m, 3H, 2, T_5', T_6), 8.22 (t, *J* = 8.0 Hz, 1H, T_4'), 8.10 (t, *J* = 8.0 Hz, 1H, T_4), 7.96 – 7.82 (m, 2H, 14, T_3"), 7.72 – 7.57 (m, 1H, 13), 7.42 (t, *J* = 6.4 Hz, 1H, T_5), 6.84 (t, *J* = 6.8 Hz, 1H, T_4"), 6.68 (t, *J* = 6.7 Hz, 1H, T_5"), 6.55 (d, *J* = 6.3 Hz, 1H, T_6"), 2.48 (s, 3H, CH_3), 2.38 (s, 3H, CH_3). ^{13}C NMR (101 MHz, [D_6]acetone) δ = 181.1 (C_q), 168.0 (C_q), 157.7 (C_q), 157.5 (C_q), 156.1 (CH, 1), 153.1 (C_H, T_6), 150.6 (C_H, 14), 149.2 (C_q), 147.8 (C_q), 147.7 (C_q), 147.4 (C_H, 7), 147.1 (C_H, 8), 140.8 (C_q), 140.1 (C_q), 139.5 (CH, T_4), 138.3 (CH, T_4'), 138.3 (C_H, T_6"), 132.8 (C_H, 12), 131.2 (C_H, 3), 130.7 (C_q), 130.5 (C_H, T_5"), 129.3 (C_q), 128.3 (C_H, T_5), 127.0 (C_H, 2), 126.6 (C_H, 13), 126.0 (C_H, T_3"), 124.7 (C_H, T_3), 123.0 (C_H, T_4"), 121.0 (C_H, T_3'), 120.3 (C_H, T_5'), 45.1 (CH_3), 43.7 (CH_3). ESI-MS: m/z calcd for $[C_{32}H_{25}N_6ORuS - PF_6]^+$: 643.1; found: 643.1; elemental analysis calcd (%) for [**3**]PF_6.4H_2O : C 44.71, H 3.87, N 9.78; found: C 43.90, H 3.48, N 9.40.

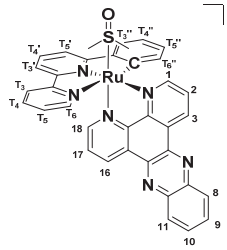

[Ru(phbpy)(dppz)(dmso)]PF_6, [**4**]PF_6: The same procedure was followed as described for [**6**]PF_6 using [Ru(dppz)(dmso)$_2$Cl$_2$] (160 mg, 0.26 mmol) and Hphbpy (60 mg, 0.26 mmol) to afford the product as a dark red powder (161 mg, 0.190 mmol, 73%). A racemic mixture was obtained but only one enantiomer is shown. ^{1}H NMR (400 MHz, [D_6]acetone) δ = 10.79 (d, *J* = 6.3 Hz, 1H, 1), 9.75 (d, *J* = 8.1 Hz, 1H, 3), 9.37 (d, *J* = 8.1 Hz, 1H, 16), 8.67 (d, *J* = 8.1 Hz, 1H, T_3), 8.53 (d, *J* = 7.9 Hz, 1H, 8), 8.48 (d, *J* = 8.3 Hz, 1H, T_3'), 8.41 – 8.29 (m,

4H, 7, 2, T_5', T_6), 8.24 (t, *J* = 8.1 Hz, 1H, T_4'), 8.20 – 8.08 (m, 3H, T_4, 9, 10), 7.87 (dd, *J* = 14.5, 6.9 Hz, 2H, 18, T_3"), 7.68 (t, *J* = 7.1 Hz, 1H, 17), 7.46 (t, *J* = 6.8 Hz, 1H, T_5), 6.88 (t, *J* = 7.5 Hz, 1H, T_4"), 6.74 (t, *J* = 7.4 Hz, 1H, T_5"), 6.66 (d, *J* = 7.5 Hz, 1H, T_6"), 2.50 (s, 3H, CH_3), 2.39 (s, 3H, CH_3). ^{13}C NMR (101 MHz, [D_6]acetone) δ = 180.3 (C_q), 167.2 (C_q), 156.8 (C_q), 156.8 (C_q), 155.4 (C_H, 1), 152.3 (C_H, T_6), 149.9 (C_H, 18), 149.4 (C_q), 148.0 (C_q), 147.1 (C_q), 142.6 (C_q), 142.4 (C_q), 140.1 (C_q), 139.5 (C_q), 138.7 (C_H, T_4), 137.7 (C_H, T_4'), 137.4 (C_H, T_6"), 132.2 (C_H, 16), 132.1 (C_H, 10), 132.1 (C_H, 11), 130.7 (C_H, 3), 130.3 (C_q), 129.8 (C_H, T_5"), 129.6 (C_H, 8), 129.5 (C_H, 9), 128.9 (C_q), 127.5 (CH, T_4), 126.3 (C_H, 2), 125.9 (C_H, 17), 125.2 (C_H, T_3"), 123.9 (C_H, T_2), 122.3 (C_H, 8), 120.2 (C_H, T_3'), 119.6 (C_H, 2), 44.3 (CH_3), 42.9 (CH_3). HRMS: m/z calcd for $[C_{36}H_{27}N_6ORuS - PF_6]^+$: 693.10105; found: 693.10113; elemental analysis calcd (%) for [**4**]PF_6: C 51.61, H 3.25, N 10.03; found: C 48.86, H 3.52, N 9.05.

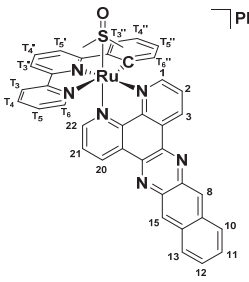

[Ru(phbpy)(dppn)(dmso)]PF_6, [**5**]PF_6: The same procedure was followed as described for [6]PF_6 using [Ru(dppn)$(dmso)_2Cl_2$] (100 mg, 0.15 mmol) and Hphbpy (35 mg, 0.15 mmol) to afford the product as a dark red powder (88 mg 0.10 mmol 65%). A racemic mixture was obtained but only one enantiomer is shown. ^{1}H NMR (500 MHz, [D_6]acetone) δ = 10.80 (d, *J* = 5.5 Hz, 1H, 1), 9.53 (d, *J* = 8.0 Hz, 1H, 3), 9.00 (d, *J* = 8.0 Hz, 1H, 20), 8.87 (s, 1H, 3), 8.71 (s, 1H, 15), 8.68 (d, *J* = 8.2 Hz, 1H, T_3), 8.54 (d, *J* = 8.0 Hz, 1H, T_3'), 8.37 (d, *J* = 7.4 Hz, 2H, T_5', T_6), 8.35 – 8.23 (m, 3H, 2, 10, T_4'), 8.14 (t, *J* = 7.9 Hz, 1H, T_4), 8.05 (d, *J* = 8.5 Hz, 1H, 13), 7.97 (d, *J* = 7.7 Hz, 1H, 3), 7.72 (d, *J* = 5.5 Hz, 1H, 22), 7.67 (t, *J* = 7.4 Hz, 1H, 12), 7.64 – 7.58 (m, 1H, 11), 7.51 – 7.44 (m, 1H, T_5), 7.38 (dd, *J* = 8.0, 5.4 Hz, 1H, 21), 6.95 (t, *J* = 7.3 Hz, 1H, T_4"), 6.87 (dt, *J* = 14.3, 7.3 Hz, 2H, T_6", T_5"), 2.52 (s, 3H, CH_3), 2.41 (s, 3H, CH_3). ^{13}C NMR (126 MHz, [D-6]acetone) δ 181.3 (C_q), 168.2 (C_q), 157.8 (C_q), 157.8 (C_q), 156.5 (C_H, 1), 153.3 (C_H, 21), 150.9 (C_q), 150.8 (C_H, 22), 149.5 (C_q), 148.1 (C_q), 141.9 (C_q), 141.3 (C_q), 139.7 (C_H, T_4), 139.3 (C_q), 139.3 (C_q), 138.9 (C_H, T_6"), 138.4 (C_H, 1), 135.9 (C_q), 135.8 (C_q), 133.0 (C_H, 20), 131.8 (C_H, 3), 131.6 (C_q), 130.9 (C_H, T_5"), 130.1(C_q) , 129.6 (C_H, 10), 129.6 (C_H, 13), 129.0 (C_H, 8), 129.0 (C_H, 15), 128.8 (C_H, 12), 128.7 (C_H, 11), 128.5 (C_H, T_5), 127.3 (C_H, 2), 126.8 (C_H, 21), 126.3 (C_H, T_3"), 124.9 (C_H, T_3), 123.4 (C_H, T_4"), 121.2 (C_H, T_3'), 120.6 (C_H, T_5'), 45.2 (CH_3), 43.9 (CH_3). HRMS: m/z calcd for $[C_{40}H_{29}N_6ORuS - PF_6]^+$: 743.11670; found: 743.11680; elemental analysis calcd (%) for [**5**]PF_6: C 54.12, H 3.29, N 9.47; found: C 52.67, H 3.82, N 8.78.

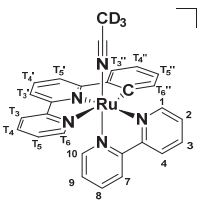

[Ru(phbpy)(bpy)(CD_3CN)]PF_6 [**6**]PF_6: [**1**]PF_6 (3.0 mg, 4.0 µmol) was dissolved in 0.6 mL deoxygenated CD_3CN and irradiated for 7 h at 1 cm from a Xenon Arc (1000 W) lamp fitted with IR (> 700 nm) and UV-cutoff (< 400 nm) filter at 298 K, while maintaining the temperature at 25 °C. After completion of the reaction, the sample was concentrated *in vacuo* to afford the title compound as a dark

purple solid (2.7 mg, 4.0 µmol, quant.). ^{1}H NMR (500 MHz, [D_3]acetonitrile) δ = 9.55 (d, *J* = 5.8 Hz, 1H, 1), 8.40 (d, *J* = 8.2 Hz, 1H, 4), 8.33 (d, *J* = 8.1 Hz, 1H, T_3), 8.18 (d, *J* = 8.1 Hz, 1H, T_3'), 8.14 (d, *J* = 8.0 Hz, 1H, T_4'), 8.03 – 7.96 (m, 3H, 3, T_6), 7.95 – 7.87 (m, 2H, T_4, T_5'), 7.74 (dd, *J* = 7.6, 1.4 Hz, 1H, T_3"), 7.68 (ddd, *J* = 7.3, 5.7, 1.4 Hz, 1H, 2), 7.58 (ddd, *J* = 8.2, 7.4, 1.5 Hz, 1H, 8), 7.36 (ddd, *J* = 5.8, 1.5, 0.8 Hz, 1H, 10), 7.32 (ddd, *J* = 7.5, 5.3, 1.2 Hz, 1H, T_5), 6.91 (ddd, *J* = 7.3, 5.8, 1.4 Hz, 1H, 9), 6.81 (td, *J* = 7.5, 1.3 Hz, 1H, T_4"), 6.73 (td, *J* = 7.3, 1.4 Hz, 1H, T_5"), 6.36 (ddd, *J* = 7.4, 1.4, 0.6 Hz, 1H, T_6"). ^{13}C NMR (126 MHz, [D_3]acetonitrile) δ = 184.8 (C_q), 167.0 (C_q), 157.2 (C_q), 156.7 (C_q), 156.7 (C_q), 154.9 (C_q), 151.0 (C_H, 1), 150.6 (C_H, T_6), 149.6 (C_H, 10), 147.8 (C_q), 137.6 (C_H, T_4), 136.3 (C_H, T_6"), 135.0 (CH, 1), 133.4 (C_H, 8), 132.5 (C_H, 3), 128.9 (C_H, T_5"), 126.7 (C_H, T_5), 125.9 (C_H, 2), 125.2 (C_H, 9), 124.4 (C_H, T_3"), 123.2 (C_H, 3), 122.8 (C_H, T_3), 122.2 (C_H, 7), 121.2 (C_H, T_4"), 118.7 (C_H, T_3'), 117.8 (C_H, 2). ESI-MS m/z calcd for $[C_{28}H_{22}N_5Ru_6 - PF_6]^+$: 530.1; found: 530.0.

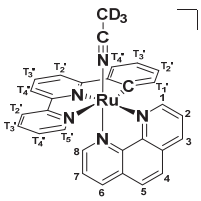

[Ru(phbpy)(phen)(CD$_3$CN)]PF$_6$, [**7**]PF$_6$: The same procedure was followed as described for [**6**]PF$_6$ using [Ru(phbpy)(bpy)(dmso)]PF$_6$ (1.9 mg, 3.0 µmol) to afford the product as a dark red solid (1.8 mg 3.0 µmol, quant.). A racemic mixture was obtained but only one enantiomer is shown. ^{1}H NMR (500 MHz, [D_3]acetonitrile) δ 9.91 (d, *J* = 4.2 Hz, 1H, 1), 8.58 (d, *J* = 7.0 Hz, 1H, 3), 8.37 (d, *J* = 7.4 Hz, 1H, T_3), 8.22 – 8.17 (m, 2H, 5, T_3'), 8.15 (d, *J* = 6.8 Hz, 1H, 8), 8.11 – 8.05 (m, 2H, 2, T_5'), 8.02 – 7.95 (m, 2H, 6, T_4'), 7.94 – 7.89 (m, 2H, T_4, T_6), 7.77 (d, *J* = 6.4 Hz, 1H, T_3"), 7.72 (d, *J* = 4.1 Hz, 1H, 10), 7.30 (dd, *J* = 8.1, 5.4 Hz, 1H, 9), 7.23 (t, *J* = 7.8, 1H, T_5), 6.78 (t, *J* = 6.8 Hz, 1H, T_4"), 6.60 (t, *J* = 7.3 Hz, 1H, T_5"), 6.17 (d, *J* = 6.2 Hz, 1H, T_6"). ^{13}C NMR (126 MHz, [D_3]acetonitrile) δ = 184.7 (C_q), 167.2 (C_q), 157.2 (C_q), 156.9 (C_q), 151.2 (C_H, 1), 150.7 (C_H, T_6), 150.1 (C_H, 10), 147.8 (C_q), 147.4 (C_q), 146.7 (C_q), 137.6 (C_H, T_4), 136.3 (C_H, T_6"), 135.1 (C_H, T_4'), 132.5 (C_H, 8), 131.5 (C_H, 3), 130.8 (C_q), 129.7 (C_q), 128.7 (C_H, T_5"), 127.7 (C_H, 5), 127.2 (C_H, 6), 126.6 (C_H, T_5), 125.2 (C_H, 2), 124.4 (C_H, T_3"), 124.1 (C_H, 9), 122.8 (C_H, T_3), 121.2 (C_H, T_4"), 118.7 (C_H, T_3'), 117.9 (C_H, 2). ESI-MS $[C_{30}H_{19}D_3N_5Ru_6 - PF_6]^+$: 559.1; found: 559.1.

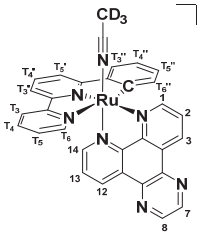

[Ru(phbpy)(dpq)(CD$_3$CN)]PF$_6$, [**8**]PF$_6$: The same procedure was followed as described for [**6**]PF$_6$ using [Ru(dpq)(dmso)$_2$Cl$_2$] (2.4 mg, 3.0 µmol) to afford the product as a dark red solid (2.2 mg, 3.0 µmol, quant.). A racemic mixture was obtained but only one enantiomer is shown. ^{1}H NMR (500 MHz, [D_3]acetonitrile) δ = 9.99 (d, *J* = 4.2 Hz, 1H, 1), 9.47 (d, *J* = 8.1 Hz, 1H, 3), 9.16 (d, *J* = 2.1 Hz, 1H, 7), 9.08 (d, *J* = 2.1 Hz, 1H, 8), 9.05 (d, *J* = 8.0 Hz, 1H, 12), 8.36 (d, *J* = 8.1 Hz, 1H, T_3), 8.22 – 8.15 (m, 2H, 2, T_3), 8.07 (d, *J* = 7.2 Hz, 1H, T_5'), 7.99 – 7.94 (m, 2H, 1, T_6), 7.91 (ddd, *J* = 8.1, 7.5, 1.6 Hz, 1H, T_4), 7.82 (d, *J* = 6.8 Hz, 1H, 14), 7.77 (d, *J* = 6.4 Hz, 1H, 3), 7.39 (dd, *J* = 8.1, 5.5 Hz, 1H, 13), 7.22 (ddd, *J* = 7.5, 5.3, 1.2 Hz, 1H, T_5), 6.77 (t, *J* = 7.3 Hz, 1H, T_4"), 6.60 (t, *J* = 7.3 Hz, 1H, T_5"), 6.28 (d, *J* = 7.4 Hz, 1H, T_6"). ^{13}C NMR (126

MHz, [D_3]acetonitrile) δ = 184.1 (C_q), 167.0 (C_q), 157.2 (C_q), 156.8 (C_q), 152.0 (C_H, 1), 151.5 (CH, T_6), 151.3 (C_H, 14), 149.1 (C_q), 148.1 (C_q), 147.8 (C_q), 146.2 (C_H, 7), 146.0 (C_H, 8), 140.4 (C_q), 140.0 (C_q), 137.8 (C_H, T_4), 136.5 (C_H, T_6''), 135.4 (C_H, T_4'), 129.8 (C_q), 129.0 (C_H, 12), 128.8 (C_H, T_5''), 128.6 (C_q), 127.9 (C_H, 3), 126.6 (C_H, T_5), 126.0 (C_H, 2), 125.1 (C_H, 13), 124.5 (C_H, T_3''), 122.9 (C_H, T_3), 121.4 (C_H, T_4''), 118.8 (C_H, T_3'), 118.0 (C_H, T_5'). ESI-MS m/z calcd for $[C_{32}H_{22}N_7Ru_6 - PF_6]^+$: 606.1; found: 606.1.

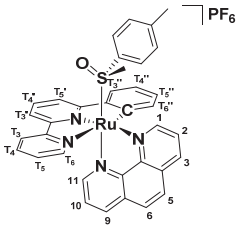

***A* and *C*-[Ru(phbpy)(phen)(*R*-methyl p-tolylsulfoxide)]PF_6, [11-*A*]PF_6 and [11-*A*]PF_6:** [**2**]PF_6 (13.6 mg, 18.5 µmol) was dissolved in deoxygenated MeCN (3 mL) and irradiated for 3 h in a custom built photo-cell 1 cm from a Xenon Arc (1000 W) lamp fitted with IR (>700 nm) and UV-cutoff (<410 nm) filter, while maintaining the temperature at 25 °C. After concentrating the reaction *in vacuo,* the resulting solid was redissolved in deoxygenated MeOH (10 mL), followed by the addition of (*R*)-(+)-methyl *p*-tolyl sulfoxide (10.3 mg, 66.8 µmol). The mixture was allowed to stir at reflux for 16 h, after it was purified over a chiral HPLC (0.1% HCO_2H, 30 to 35% MeCN in H_2O, 20 min) affording both [**11-C**]PF_6 (R_f = 12.184 min, 0.8 mg, 0.99 µmol, 5%) and [**11-A**]PF_6 (R_f = 12.984 min, 0.5 mg, 0.62 µmol, 3%) as their respective diastereomers, [**11-A**]PF_6: ^{1}H NMR (850 MHz, [D_3]acetonitrile) δ = 10.75 (d, *J* = 5.3 Hz, 1H, 1), 8.67 (d, *J* = 8.2 Hz, 1H, 3), 8.32 (d, *J* = 7.9 Hz, 1H, T_2'), 8.20 (d, *J* = 8.8 Hz, 1H, 5), 8.16 (dd, *J* = 8.2, 5.2 Hz, 1H, 2), 8.03 (d, *J* = 8.8 Hz, 1H, 6), 8.00 (d, *J* = 8.1 Hz, 1H, 11), 7.89 – 7.86 (m, 2H, 10, T_5), 7.84 (d, *J* = 5.3 Hz, 1H, T_2), 7.80 – 7.75 (m, 2H, T_4'', T_4), 7.72 (d, *J* = 8.0 Hz, 1H, 9), 7.47 (d, *J* = 5.4 Hz, 1H, T_4'), 7.40 (dd, *J* = 8.1, 5.2 Hz, 1H, T_3'), 7.14 (dd, *J* = 7.3, 5.4 Hz, 1H, T_3), 6.89 (t, *J* = 7.3 Hz, 1H, T_3''), 6.81 (d, *J* = 8.1 Hz, 2H, 2 x CH *m*-tolyl), 6.71 (t, *J* = 7.2 Hz, 1H, T_2''), 6.44 (d, *J* = 7.5 Hz, 1H, T_1''), 6.43 (d, *J* = 12.9, 7.8 Hz, 2H, 2 x CH *o*-tolyl), 2.77 (s, 3H). ESI-MS m/z calcd for $[C_{36}H_{29}N_4ORuS - PF_6]^+$: 667.1; found: 667.1.

5.5.3 Photochemistry

5.5.3.1 Photosubstitution quantum yield

3.00 mL of [**1**]PF_6 (6.83 x 10^{-5} M), [**2**]PF_6 (4.10 x 10^{-5} M), [**3**]PF_6 (4.10 x 10^{-5} M) or [**9**]$(PF_6)_2$ (6.52 x 10^{-5} M) in acetonitrile was transferred to a 1 cm wide quartz fluorescence cuvette with stirring bar and deoxygenated for 15 minutes with dinitrogen after which it was irradiated with a Roithner LaserTechnik H2A1-H450 LED (λ_{exc} 450 nm, FWHM 35 nm) with photon flux Φ = 1.86 · mol photons · s^{-1} (or Φ = 1.86 · mol photons · s^{-1} for [**9**]$(PF_6)_2$) while the solution was kept at constant temperature (25° C). During this period UV-vis spectra were recorded on a Varian Inc. Cary 50 UV-vis spectrometer with an interval of 10 minutes for 24 h and ESI-MS spectra were recorded after the irradiation experiment to confirm the formation of the solvent species $[Ru(phbpy)(N\text{-}N)(MeCN)]^+$. Photosubstitution quantum yields were determined as described earlier.[36]

5.5.3.2 NMR irradiation experiments

^{1}H NMR irradiation experiments were carried out as follows: 2.0 mg of either [**1**]PF_6, [**2**]PF_6 or [**3**]PF_6 were dissolved in 0.6 mL [D_3]acetonitrile and irradiated 1 cm from a Xenon-Arc 1000 W fitted with IR (>700 nm) and UV-cutoff (<410 nm) filters, while maintaining the temperature at 25 °C during the irradiation period spectra were recorded every h on a Bruker AV-400 until completion.

5.5.3.3 Singlet oxygen quantum yield

Singlet oxygen measurements were carried out as described in the appendix (II.1).

5.5.4 Electrochemistry

Cyclic voltammetry experiments were performed using a cell with a platinum working electrode, a silver wire as pseudo-reference electrode, and a platinum wire as auxiliary electrode. 0.1 M Bu_4NPF_6 in MeCN was used as the supporting electrolyte. 1 mM solutions of each complex were purged with argon prior to the experiment, and was measured at room temperature using Autolab PGSTAT10 and GPES 4.9 by Eco Chemie. Each experiment was calibrated against ferrocene with a scan rate of 100 mV s^{-1}. For [**4**]PF_6, [**6**]PF_6**,** [**7**]PF_6**,** [**8**]PF_6 a scan rate of 200 mV s^{-1} was used.

5.5.5 DNA-interactions

Agarose gel electrophoresis was carried out as described in appendix II.2.2 according to the following table for compound [**1**]PF_6 – [**3**]PF_6:

Lane	Description	Time of irradiation (min)	Light dose (Jcm^{-2})
1	λ MW marker	0	0
2	DNA control, 37 °C, dark	0	0
3	DNA control, 37 °C, irradiated	15	22.5
4	5:1 BP:MC, 37 °C, dark	0	0
5	5:1 BP:MC, 37 °C, irradiated 1 min	1	1.5
6	5:1 BP:MC, 37 °C, irradiated 3 min	3	4.5
7	5:1 BP:MC, 37 °C, irradiated 5 min	5	7.5
8	5:1 BP:MC, 37 °C, irradiated 10 min	10	15
9	5:1 BP:MC, 37 °C, irradiated 15 min	15	22.5
10	λ MW marker	0	0

For compound [**5**]PF_6 the following table was used:

Lane	BP:MC
1	Cisplatin control
2	DNA control
3	5
4	10
5	15
6	25
7	50
8	100
9	λ MW marker

5.5.6 Cytotoxicity Assay

The cytotoxicity assay was carried out as described in appendix II.2.1 with the following modifications: Compounds [**1**]PF_6 – [**3**]PF_6 were directly diluted in OptiMEM medium. For compounds [**4**]PF_6 and [**5**]PF_6 DMSO needed to be added, but final DMSO concentrations did not exceed 0.5%. Compounds [**1**]PF_6 – [**3**]PF_6 were irradiated for 10 minutes with green light (520 ± 38 nm, 25.0 ± 1.9 mW cm^{-2}, 10 minutes, 15 · ± 1.2 J cm^{-2}).

5.5.7 Circular Dichroism

Measurements were performed on a BioLogic Science Instruments MOS-500 Circular Dichroism Spectrometer, using stock solutions of 4.9 x 10^{-5} M for both [**11-A**] and [**11-C**] in acetonitrile.

References

[1] a). B. S. Murray, M. V. Babak, C. G. Hartinger, P. J. Dyson, *Coord Chem Rev* **2016**, *306*, 86-114; b). S. J. Dougan, P. J. Sadler, *Chimia* **2007**, *61*, 704-715.

[2] B. Pena, A. David, C. Pavani, M. S. Baptista, J. P. Pellois, C. Turro, K. R. Dunbar, *Organometallics* **2014**, *33*, 1100-1103.

[3] C. Mari, V. Pierroz, R. Rubbiani, M. Patra, J. Hess, B. Spingler, L. Oehninger, J. Schur, I. Ott, L. Salassa, S. Ferrari, G. Gasser, *Chem Eur J* **2014**, *20*, 14421-14436.

[4] E. Wachter, D. K. Heidary, B. S. Howerton, S. Parkin, E. C. Glazer, *Chem Commun* **2012**, *48*, 9649-9651.

[5] H. Chan, J. B. Ghrayche, J. Wei, A. K. Renfrew, *Eur J Inorg Chem* **2017**, *2017*, 1679-1686.

[6] B. A. Albani, B. Pena, N. A. Leed, N. A. de Paula, C. Pavani, M. S. Baptista, K. R. Dunbar, C. Turro, *J Am Chem Soc* **2014**, *136*, 17095-17101.

[7] J. Liu, L. N. Ji, W. J. Mei, *Prog Chem* **2004**, *16*, 969-974.

[8] H. Y. Huang, P. Y. Zhang, H. M. Chen, L. N. Ji, H. Chao, *Chem Eur J* **2015**, *21*, 715-725.

[9] U. Schatzschneider, J. Niesel, I. Ott, R. Gust, H. Alborzinia, S. Wolfl, *ChemMedChem* **2008**, *3*, 1104-1109.

[10] C. Mari, V. Pierroz, S. Ferrari, G. Gasser, *Chem Sci* **2015**, *6*, 2660-2686.

[11] T. Funaki, M. Yanagida, N. Onozawa-Komatsuzaki, K. Kasuga, Y. Kawanishi, M. Kurashige, K. Sayama, H. Sugihara, *Inorg Chem Commun* **2009**, *12*, 842-845.

[12] A. M. Palmer, B. Pena, R. B. Sears, O. Chen, M. El Ojaimi, R. P. Thummel, K. R. Dunbar, C. Turro, *Philos T R Soc A* **2013**, *371*, 20120135.

[13] A. D. Ryabov, R. Le Lagadec, H. Estevez, R. A. Toscano, S. Hernandez, L. Alexandrova, V. S. Kurova, A. Fischer, C. Sirlin, M. Pfeffer, *Inorg Chem* **2005**, *44*, 1626-1634.

[14] S. Bonnet, J. P. Collin, N. Gruber, J. P. Sauvage, E. R. Schofield, *Dalton Trans* **2003**, 4654-4662.

[15] J. J. Rack, J. R. Winkler, H. B. Gray, *J Am Chem Soc* **2001**, *123*, 2432-2433.

[16] B. A. Albani, B. Pena, K. R. Dunbar, C. Turro, *Photobiol Sci* **2014**, *13*, 272-280.

[17] F. Barigelletti, B. Ventura, J. P. Collin, R. Kayhanian, P. Gavina, J. P. Sauvage, *Eur J Inorg Chem* **2000**, 113-119.

[18] J. P. Collin, M. Beley, J. P. Sauvage, F. Barigelletti, *Inorg Chim Acta* **1991**, *186*, 91-93.

[19] a). L. N. Lameijer, S. L. Hopkins, T. G. Breve, S. H. Askes, S. Bonnet, *Chem Eur J* **2016**, *22*, 18484-18491; b). J. D. Knoll, B. A. Albani, C. B. Durr, C. Turro, *J Phys Chem A* **2014**, *118*, 10603-10610.

[20] R. E. Goldbach, I. Rodriguez-Garcia, J. H. van Lenthe, M. A. Siegler, S. Bonnet, *Chem Eur J* **2011**, *17*, 9924-9929.

[21] H. J. Jang, S. L. Hopkins, M. A. Siegler, S. Bonnet, *Dalton Trans* **2017**, *46*, 9969-9980.

[22] J. J. Rack, A. A. Rachford, A. M. Shelker, *Inorg Chem* **2003**, *42*, 7357-7359.

[23] S. P. Foxon, C. Metcalfe, H. Adams, M. Webb, J. A. Thomas, *Inorg Chem* **2007**, *46*, 409-416.

[24] T. A. White, S. Maji, S. Ott, *Dalton Trans* **2014**, *43*, 15028-15037.

[25] J. D. Knoll, B. A. Albani, C. Turro, *Acc Chem Res* **2015**, *48*, 2280-2287.

[26] B. Laleu, P. Mobian, C. Herse, B. W. Laursen, G. Hopfgartner, G. Bernardinelli, J. Lacour, *Angew Chem Int Ed* **2005**, *44*, 1879-1883.

[27] A. J. Gottle, F. Alary, M. Boggio-Pasqua, I. M. Dixon, J. L. Heully, A. Bahreman, S. H. Askes, S. Bonnet, *Inorg Chem* **2016**, *55*, 4448-4456.

[28] V. Vichai, K. Kirtikara, *Nat Protocols* **2006**, *1*, 1112-1116.

[29] L. Fetzer, B. Boff, M. Ali, M. Xiangjun, J. P. Collin, C. Sirlin, C. Gaiddon, M. Pfeffer, *Dalton Trans* **2011**, *40*, 8869-8878.

[30] a). V. Pierroz, R. Rubbiani, C. Gentili, M. Patra, C. Mari, G. Gasser, S. Ferrari, *Chem Sci* **2016**, *7*, 6115-6124; b). H. Song, J. T. Kaiser, J. K. Barton, *Nat Chem* **2012**, *4*, 615-620; c). Y. Sun, L. E. Joyce, N. M. Dickson, C. Turro, *Chem Commun* **2010**, *46*, 2426-2428; d). H. Huang, P. Zhang, B. Yu, Y. Chen, J. Wang, L. Ji, H. Chao, *J Med Chem* **2014**, *57*, 8971-8983.

[31] E. B. van der Tol, H. J. van Ramesdonk, J. W. Verhoeven, F. J. Steemers, E. G. Kerver, W. Verboom, D. N. Reinhoudt, *Chem Eur J* **1998**, *4*, 2315-2323.

[32] Z. Molphy, A. Prisecaru, C. Slator, N. Barron, M. McCann, J. Colleran, D. Chandran, N. Gathergood, A. Kellett, *Inorg Chem* **2014**, *53*, 5392-5404.

[33] E. C. Constable, R. P. Henney, T. A. Leese, D. A. Tocher, *Dalton Trans* **1990**, 443-449.

[34] M. L. Bode, P. J. Gates, S. Y. Gebretnsae, R. Vleggaar, *Tetrahedron* **2010**, *66*, 2026-2036.

[35] I. P. Evans, A. Spencer, W. G, *J Chem Soc Dalton* **1973**, 204-209.

[36] A. Bahreman, J. A. Cuello-Garibo, S. Bonnet, *Dalton Trans* **2014**, *43*, 4494-4505.